Balance and tropical data assimilation

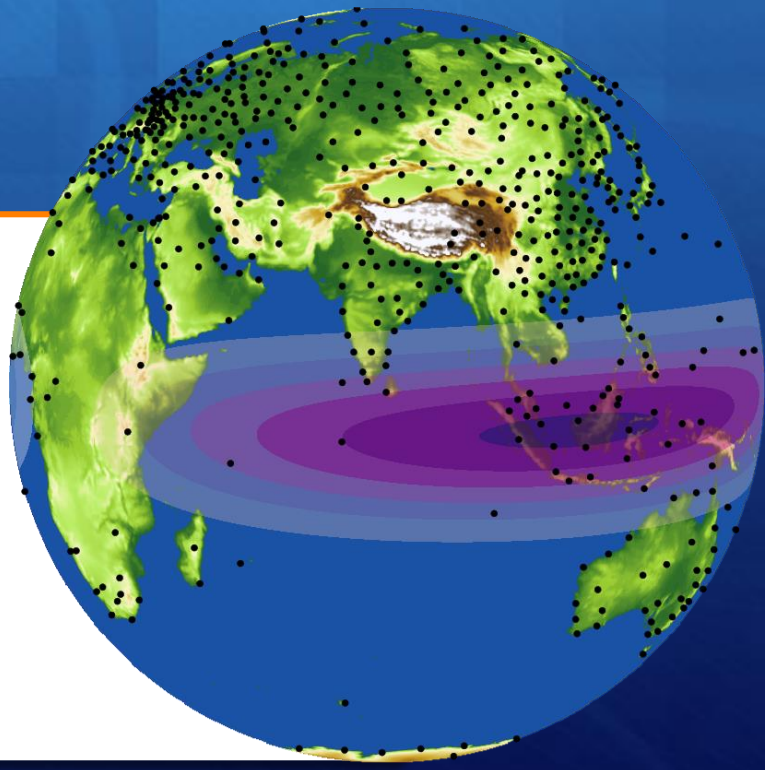

Nedjeljka Žagar
University of Ljubljana, Slovenia

Outline

- Tropical analysis uncertainties and the growth of tropical forecast uncertainties in a global perspective
- Modelling of the tropical forecast-error covariances
- Scale-dependent and flow-dependent growth of tropical forecast errors
- Impact of model error
- Conclusions and outlook

1. Analysis uncertainties and the growth of forecast uncertainties in IFS

Zonally-averaged ensemble spread in EDA

3-hour ensemble spread in the zonal wind, cy32r3

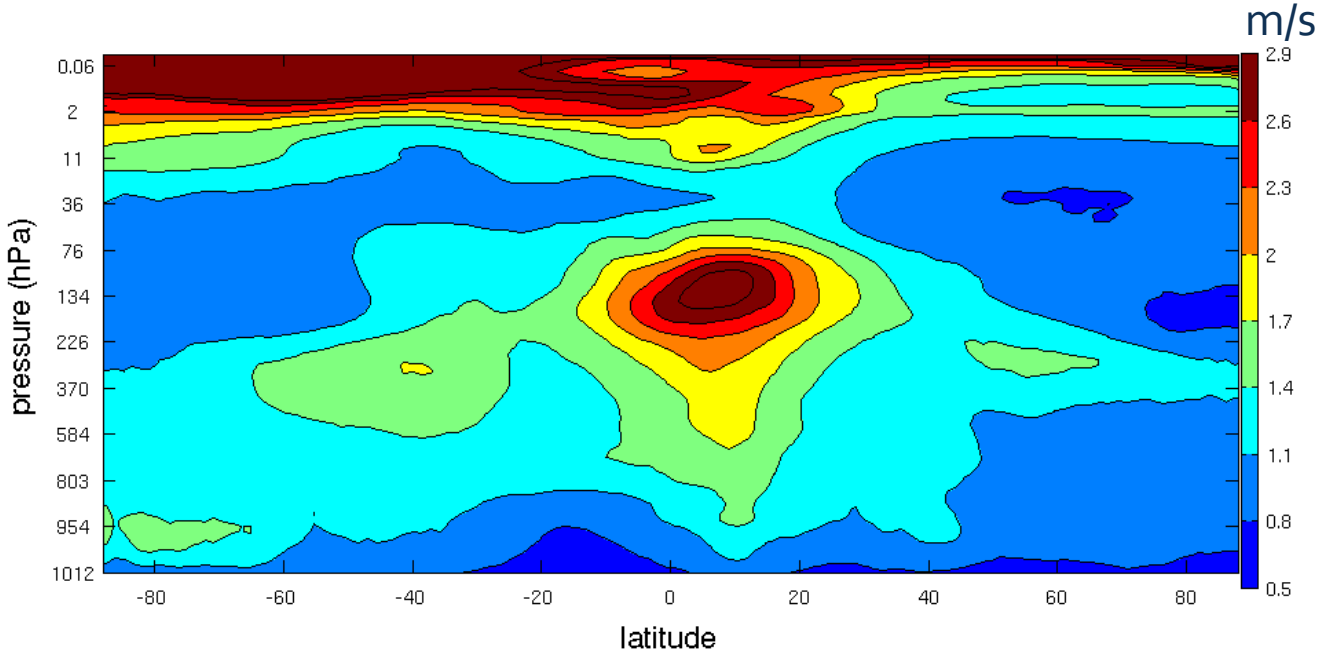

Žagar et al., 2013, QJRMS

Zonally-averaged growth of forecast uncertainties in ENS

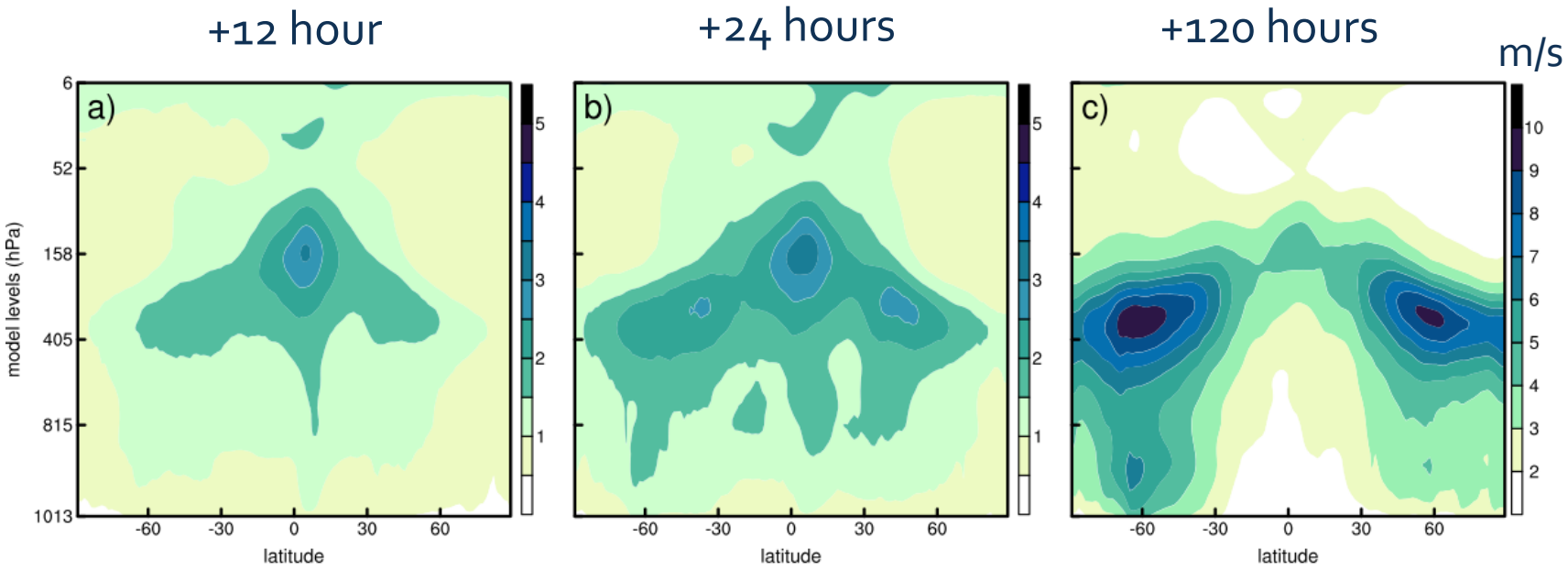

ECMWF ensemble prediction system: two weeks of data in May 2015
Ensemble spread in zonal wind (m/s)

Žagar et al., 2016, Tellus

Global growth of forecast uncertainties

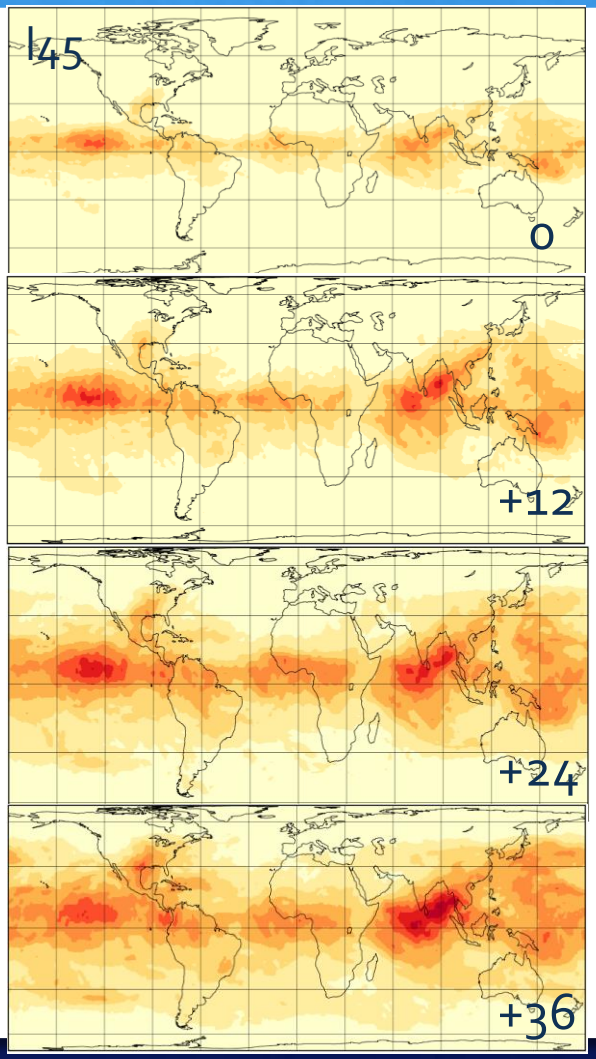

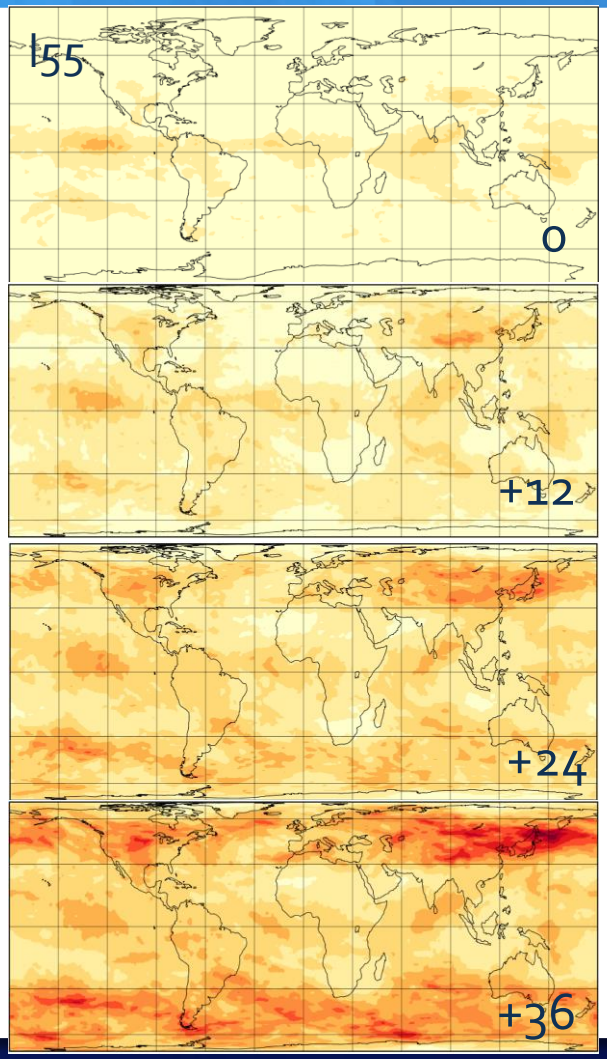

ENS data
Two weeks in May 2015

Ensemble spread in zonal wind (m/s)

lev55, ~290 hPa

lev45, ~150 hPa

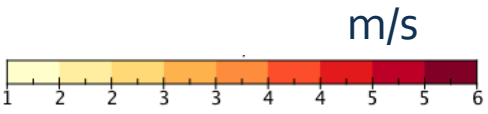

Global analysis and forecast uncertainties

Initial-state uncertainties are largest in the tropics

How do the forecast uncertainties grow as a function of scale?

How the growth depends on dynamics (balanced versus unbalanced)?

How the forecast errors in medium range in the mid-latitudes depend on the tropical analysis uncertainties?

We take a global, 3D view of forecast errors as represented by the ensemble spread of operational ensemble forecasts of ECMWF

Uncertainties in tropical winds: ERA Interim vs. MERRA reanalyses

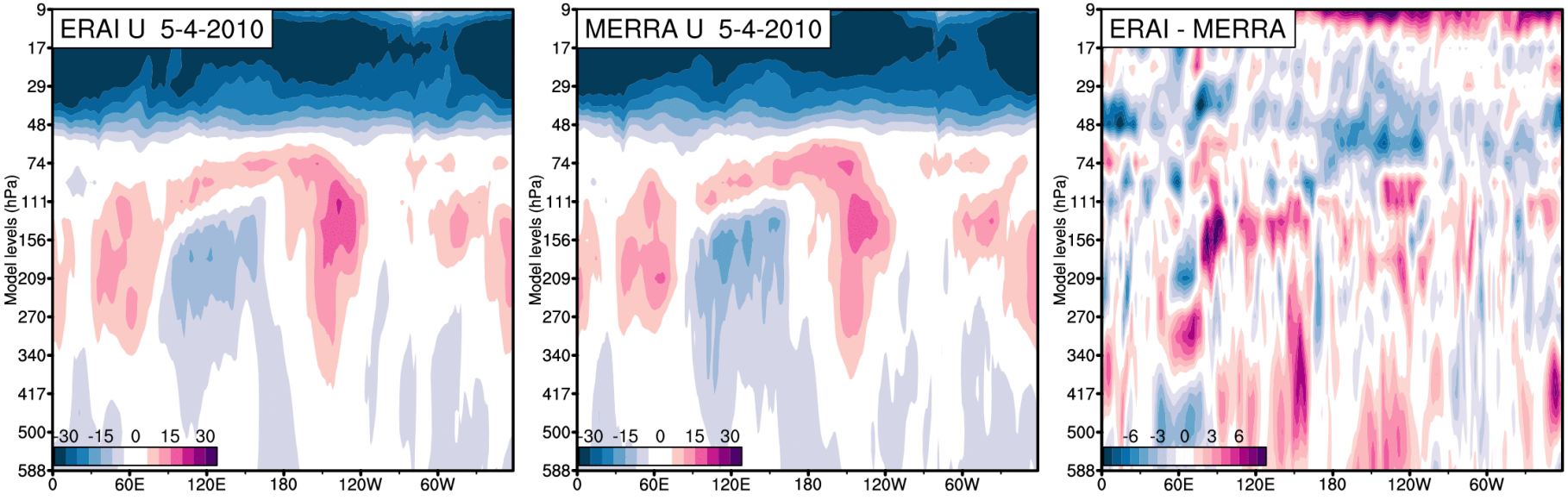

Zonal wind averaged between 5°N and 5° S
PreConcordiasi period in April 2010 with the balloon measurements
(talks by A. Hertzog and R. Plougonven)

Uncertainties in tropical Kelvin wave: ERA Interim vs. MERRA reanalyses

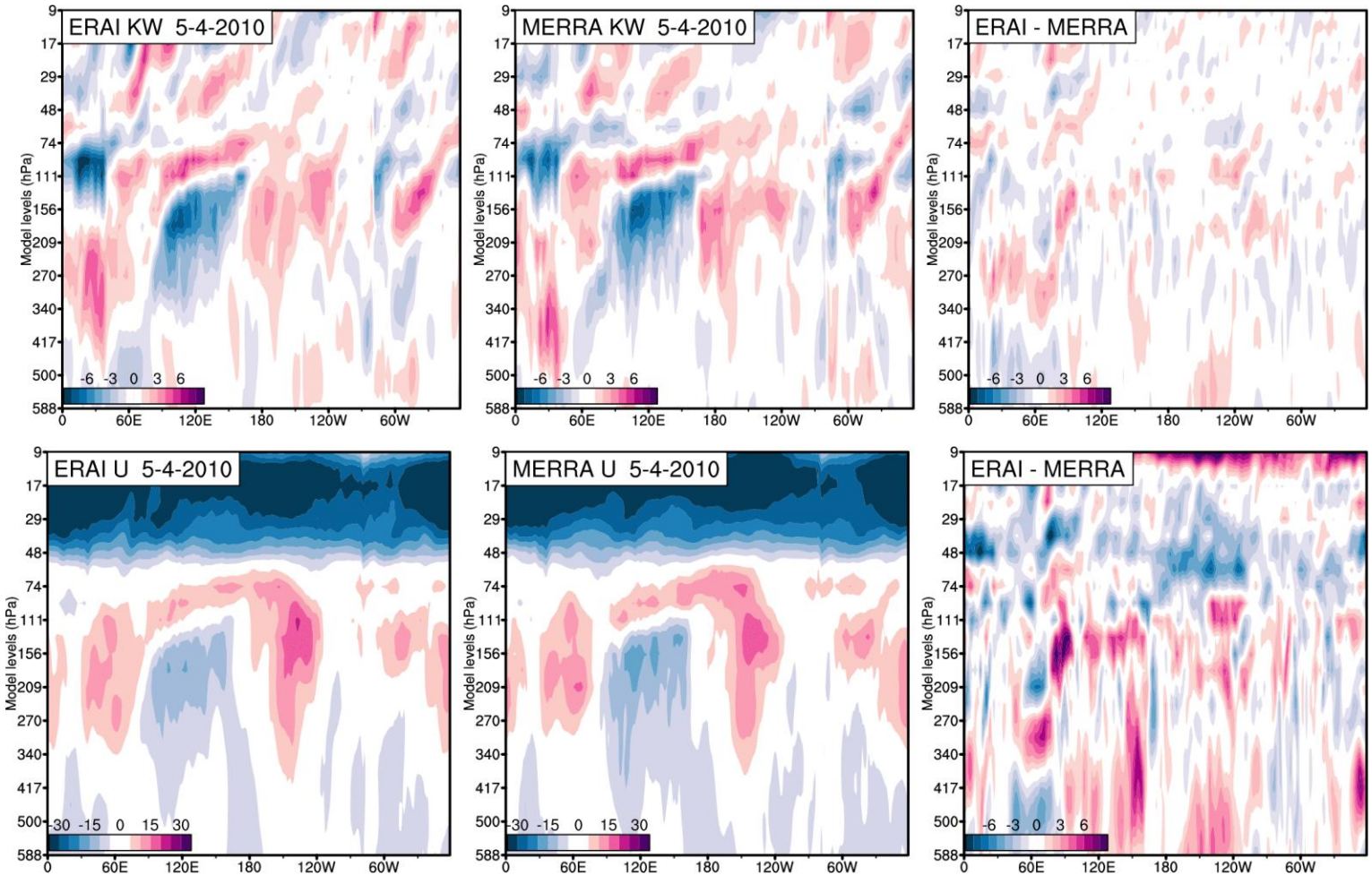

Uncertainties in tropical Kelvin wave: ERA Interim vs. MERRA reanalyses

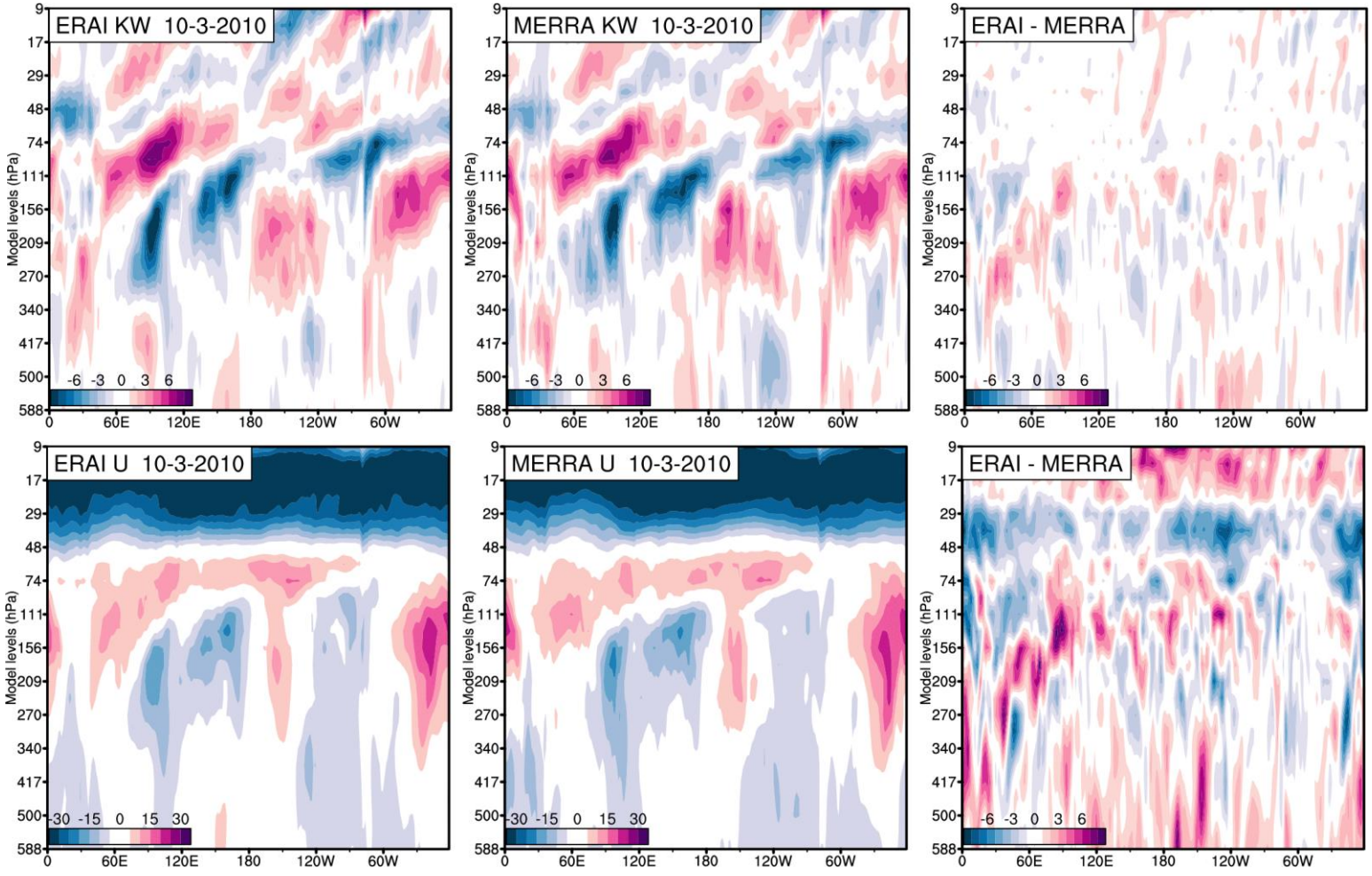

2. Modelling the tropical forecast-error covariances

Multivariate decomposition of global data using the Hough harmonics

Solutions in terms of horizontal and vertical dependencies:

$$[u', v', h']^{\mathsf{T}}(\lambda, \phi, \sigma, t) = [u, v, h]^{\mathsf{T}}(\lambda, \phi, t) \times G(\sigma)$$

$$\mathbf{X}(l, j, s_j) = \sum_{m=1}^{M} \mathbf{S}_m \mathbf{X}_m(l, j) \times G_m(j)$$

$$\mathbf{X}_m(l, j) = \sum_{n=1}^{R} \sum_{k=-K}^{K} c_n^k(m) \mathbf{H}_n^k(l, j, m)$$

Two kinds of Hough harmonic solutions for the horizontal wave motions

Frequencies of spherical normal modes for different equivalent depths

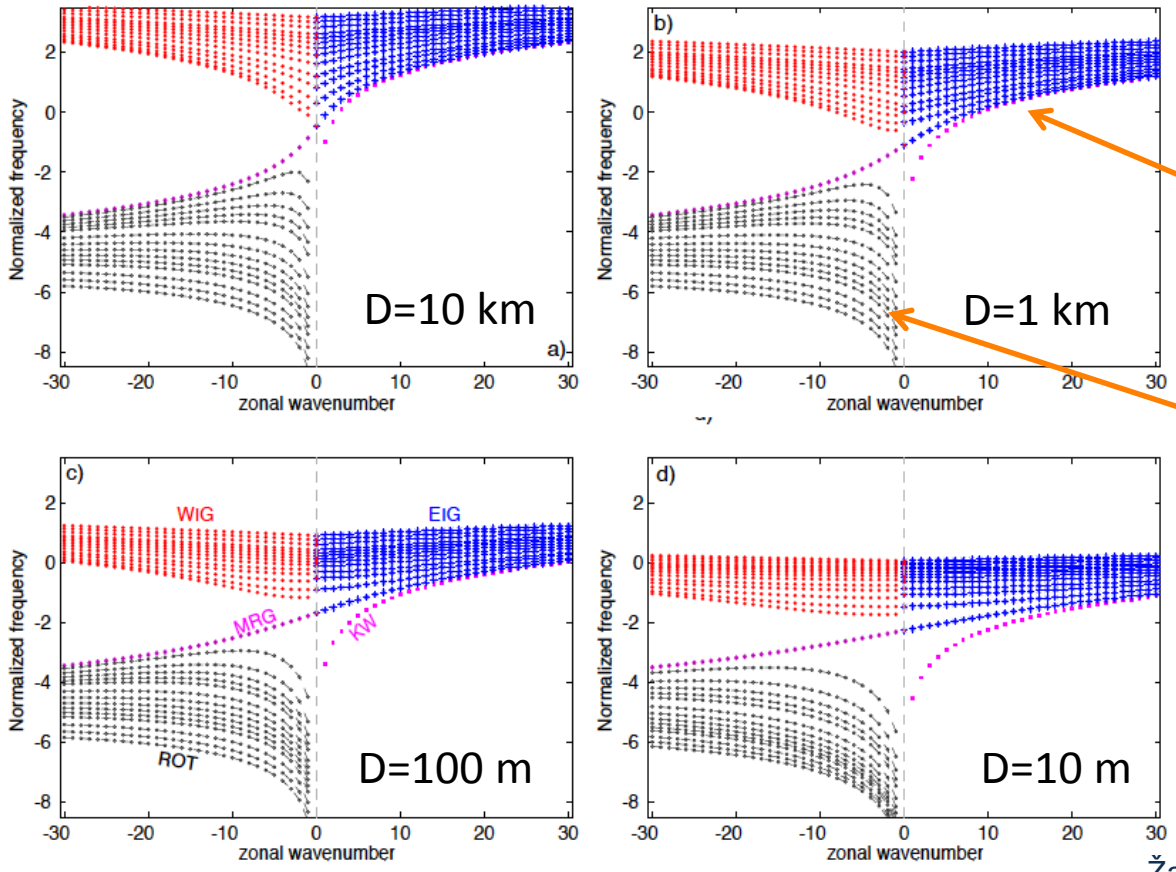

Unbalanced Or Inertio-gravity

Balanced Or Rossby-type

Žagar et al., 2015, GMD

Meridional structure of Hough functions

HSFs are pre-computed for a given number of vertical modes, M

For every m=1,…,M, i.e. for every D_m

Meridional structure for Hough functions is computed for a range of the zonal wavenumbers K,

k=-K,..,0,…,K

and a range of meridional modes for the balanced, N_{ROSSBY}, a range of EIG, N_{EIG}, and a range of WIG, N_{WIG}, modes.

$R=N_{ROSSBY} + N_{EIG} + N_{WIG}$

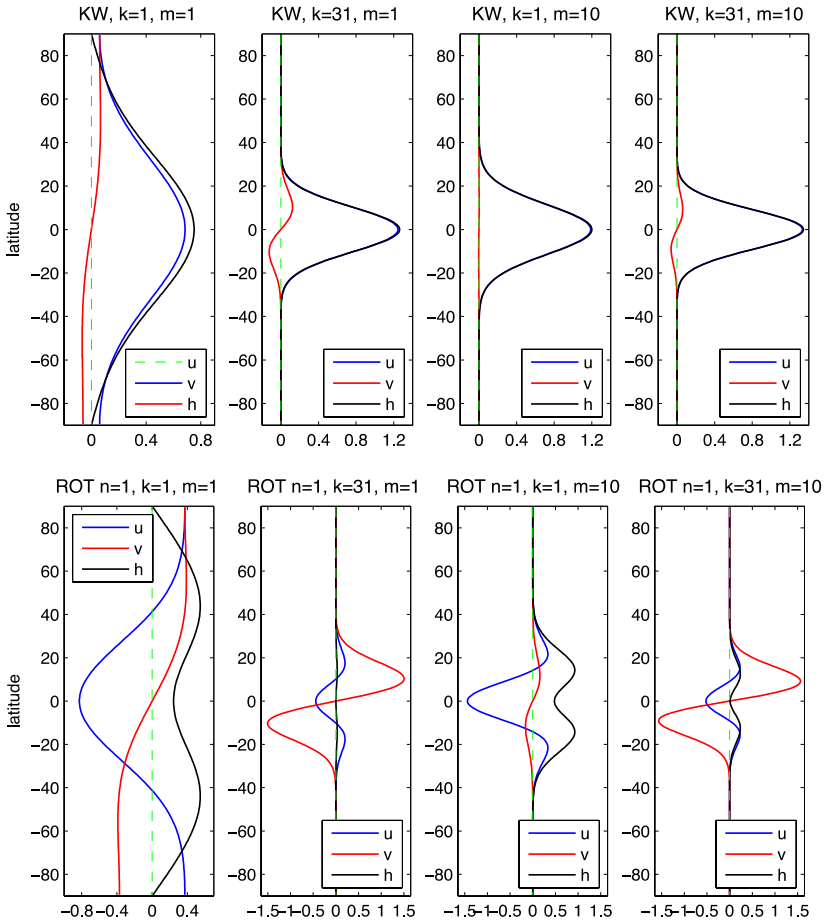

Žagar et al., 2015, GMD

History of Hough functions in data assimilation (1)

- Flattery, 1970s: NCEP OI based on the Hough functions
- D. Parrish, mid 1980s: computed correlations for single point in the tropics including the impact of KW and MRG waves

Single height observations at EQ

Parrish, 1988, AMS proceedings

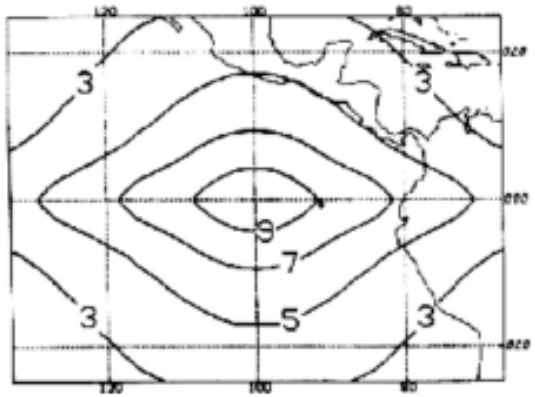

(h,h), Rossby+MRG

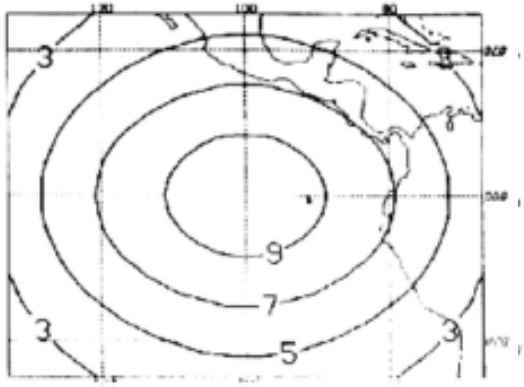

(h,h), Rossby+MRG+KW, k=1-3

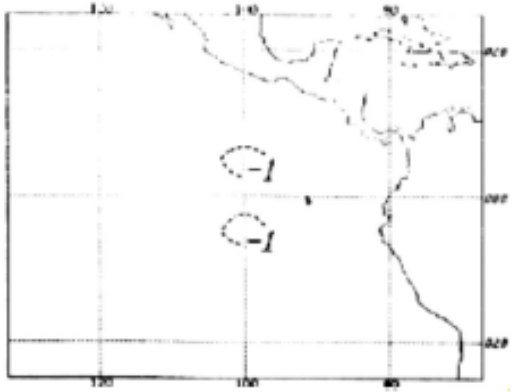

(h,u), Rossby+MRG+KW, k=1-3

History of Hough functions in data assimilation (2)

- ECMWF, early 1990s: first formulation of 3D-Var used Hough functions

$$J_b = \tfrac{1}{2}\, c_R\, \chi_R^t\, \Lambda_R^{-1}\, \chi_R + \tfrac{1}{2}\, c_G\, \chi_G^t\, \Lambda_G^{-1}\, \chi_G + \tfrac{1}{2}\, \chi_U^t\, \Lambda_U^{-1}\, \chi_U$$

c_G is set to $\frac{1}{2\varepsilon}$ and c_R to $\frac{1}{2(1-\varepsilon)}$

Heckley et al., 1993, ECMWF proceedings

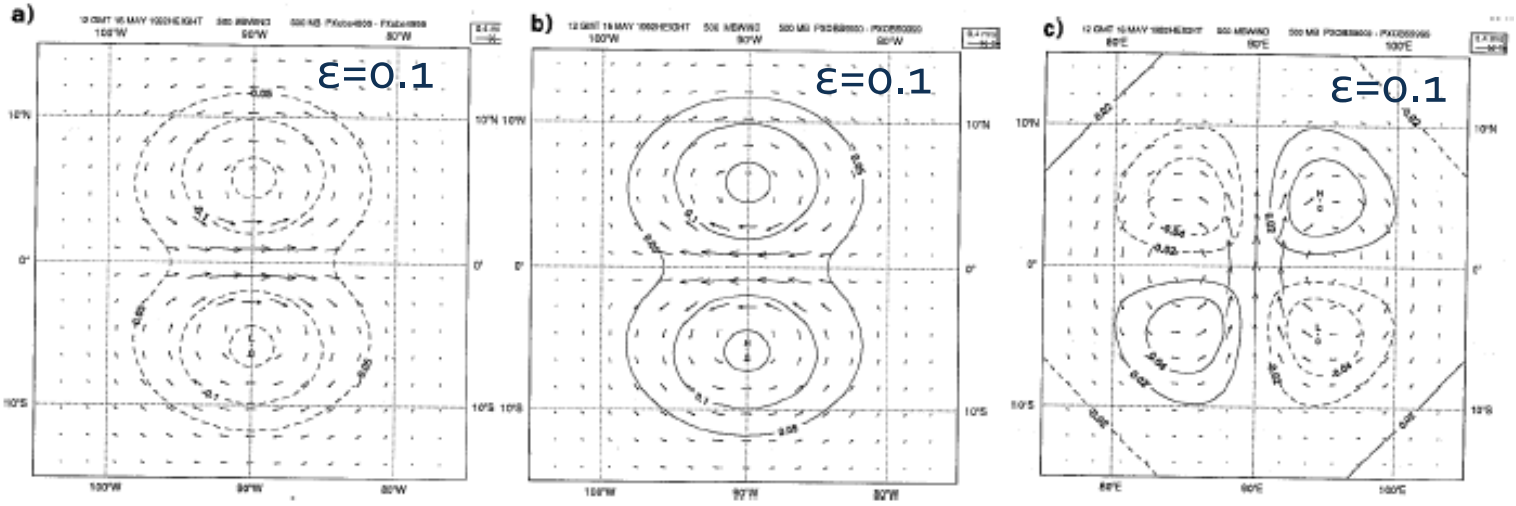

Single westerly wind obs at the EQ

Single easterly wind obs at the EQ

Single southerly wind obs at the EQ

History of Hough functions in data assimilation (3)

- ECMWF, early 1990s: first formulation of 3D-Var used Hough functions

$$J_b = \tfrac{1}{2}\, c_R\, \chi_R^t\, \Lambda_R^{-1}\, \chi_R + \tfrac{1}{2}\, c_G\, \chi_G^t\, \Lambda_G^{-1}\, \chi_G + \tfrac{1}{2}\, \chi_U^t\, \Lambda_U^{-1}\, \chi_U$$

c_G is set to $\frac{1}{2\varepsilon}$ and c_R to $\frac{1}{2(1-\varepsilon)}$

Heckley et al., 1993, ECMWF proceedings

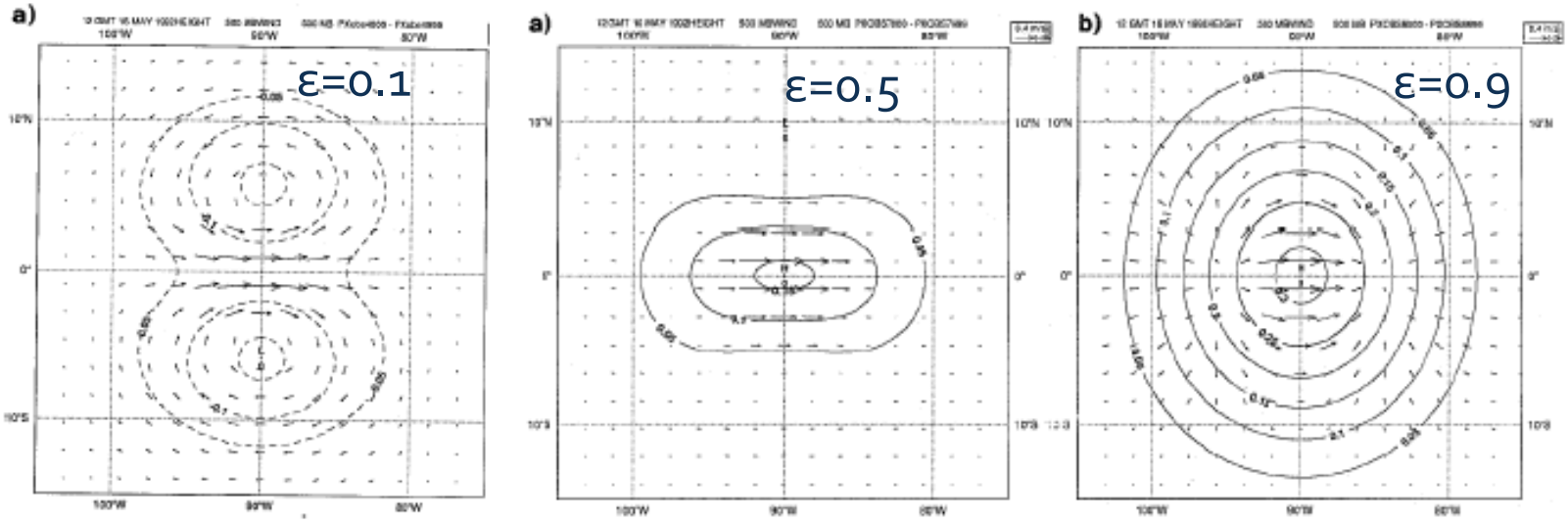

Single westerly wind obs at the EQ at 500 hPa

Tropical data assimilation system including Rossby and IG wave constraints

- Application of parabolic cylinder functions as the basis functions for the representation of the background-error covariances

Daley, 1993, Atm.-Ocean; Žagar et al., 2004, QJRMS

$$J(\delta\mathbf{x}) = J_b + J_o = \frac{1}{2}\delta\mathbf{x}^{\mathrm{T}}\mathbf{B}^{-1}\delta\mathbf{x} + \frac{1}{2}\sum_{n=1}^{K}\left(\mathbf{y}_n - \mathrm{H}\left(\mathbf{x}^b + \delta\mathbf{x}_n\right)\right)^{\mathrm{T}}\mathbf{R}^{-1}\left(\mathbf{y}_n - \mathrm{H}\left(\mathbf{x}^b + \delta\mathbf{x}_n\right)\right)$$

$$J(\chi) = J_b + J_o = \frac{1}{2}\chi^{\mathrm{T}}\chi + \frac{1}{2}\sum_{n=1}^{K}\left(\mathbf{y}_n - \mathrm{H}\left(\mathbf{x}^b + \mathbf{L}^{-1}\chi_n\right)\right)^{\mathrm{T}}\mathbf{R}^{-1}\left(\mathbf{y}_n - \mathrm{H}\left(\mathbf{x}^b + \mathrm{L}^{-1}\chi_n\right)\right)$$

$$\chi = L\delta\mathbf{x}$$

$$\mathrm{L} = \mathrm{DP_yF_xF^{-1}}$$

P_y – projection operator on the meridionally dependent part of equatorial eigenmodes

D – spectral variance density normalization

F – Fourier transform operator

Distribution of tropical forecast-error variance among equatorial modes

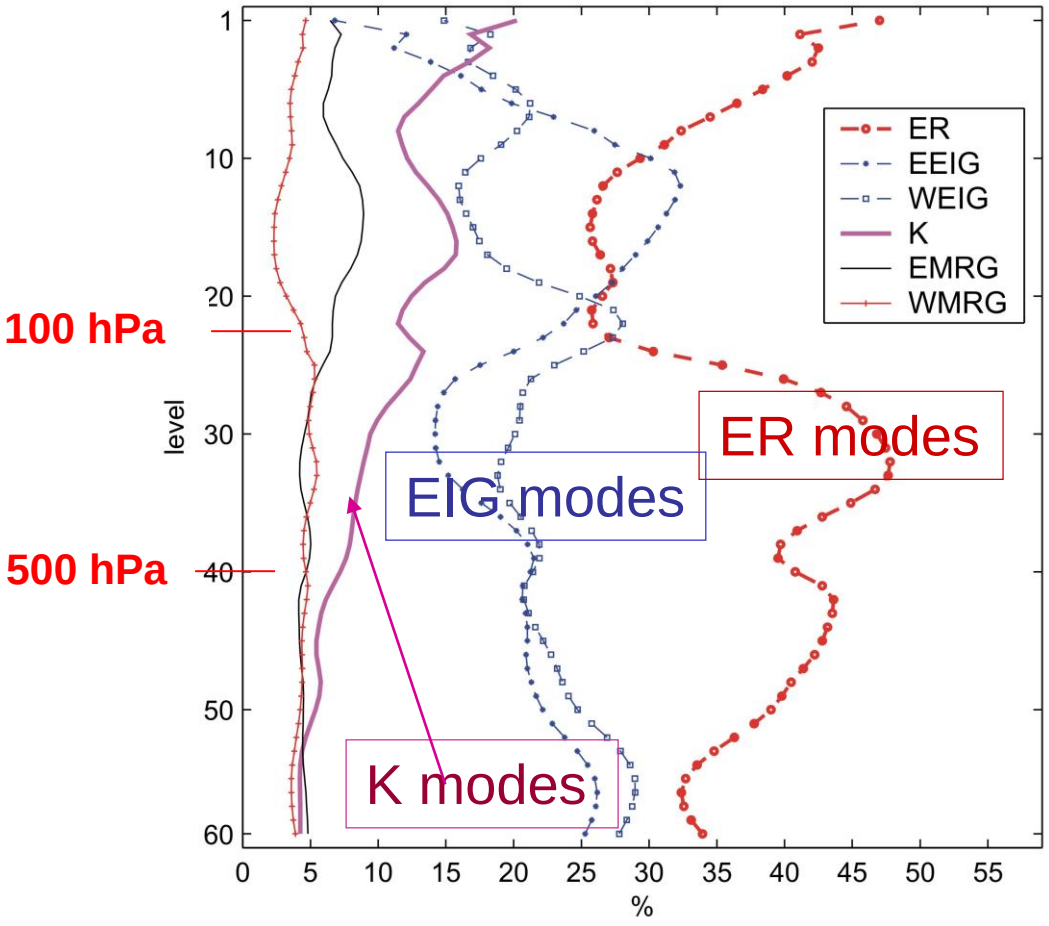

Dataset from October 2000
10 member ensemble
Perturbed obs

Parabolic cylinder functions as basis functions applied on each level
Equatorial belt 20S-20N

Žagar et al., QJRMS 2005

Impact of the equatorial wave constraint on analysis increments

Single h observations at the equator

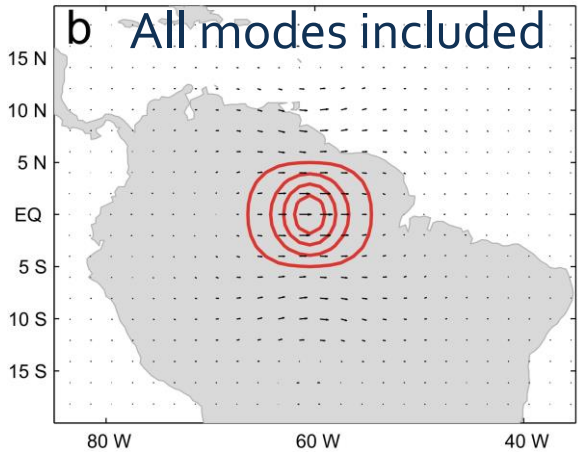

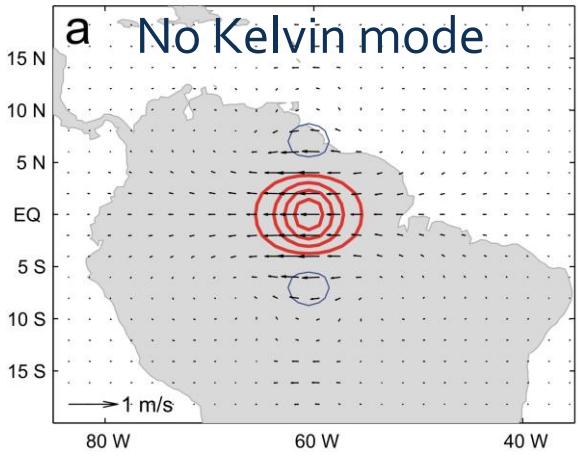

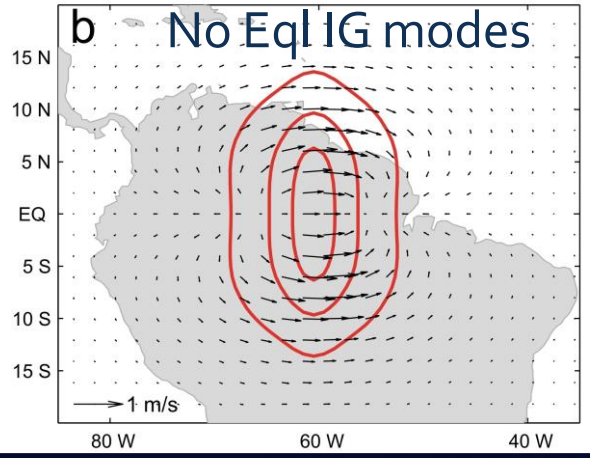

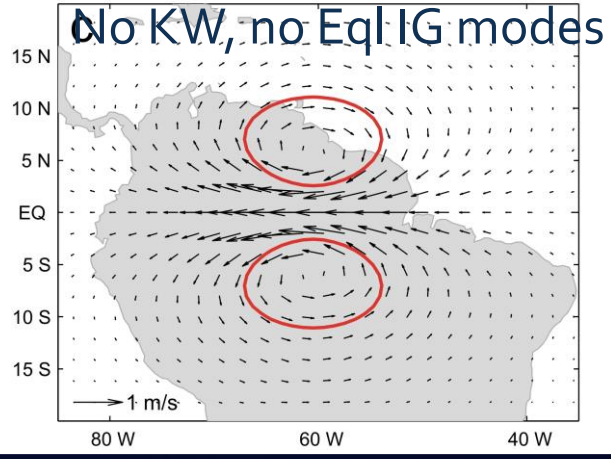

Kelvin wave coupling is decisive for the structure of analysis increments near the equator

EIG waves reduce the meridional correlation scale, and also effect the mass/wind coupling

Žagar et al., 2004, QJRMS

Impact of the equatorial wave constraint on analysis increments

Single westerly wind obs at the EQ

Rossby waves

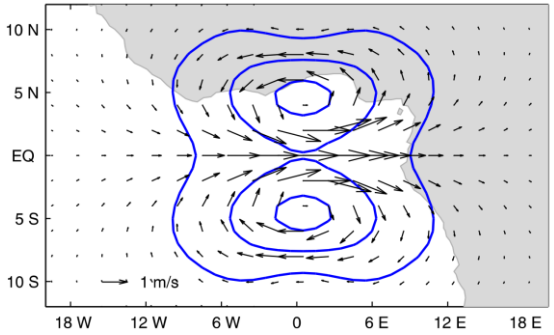

Rossby, KW, MRG

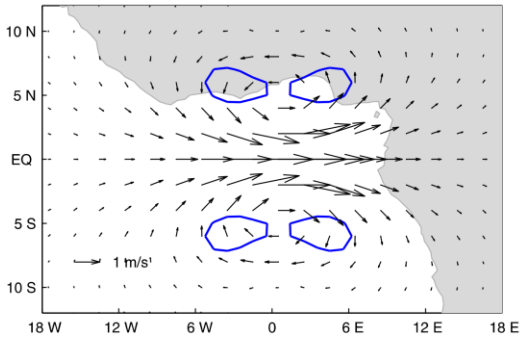

All waves

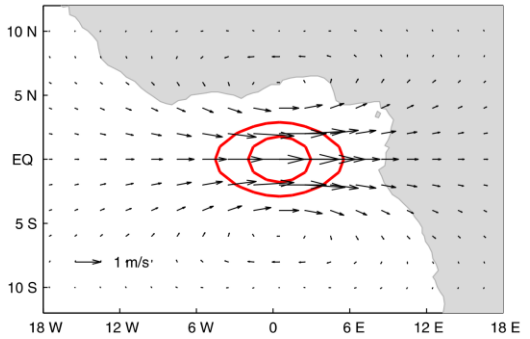

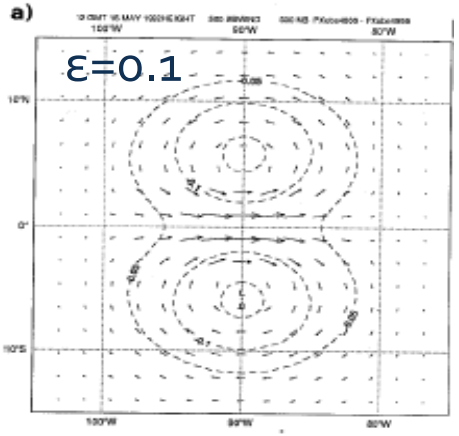

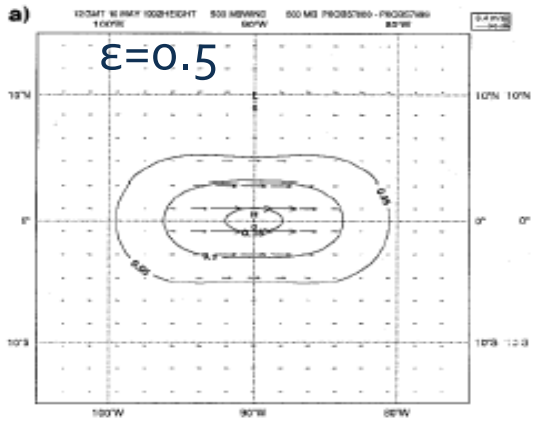

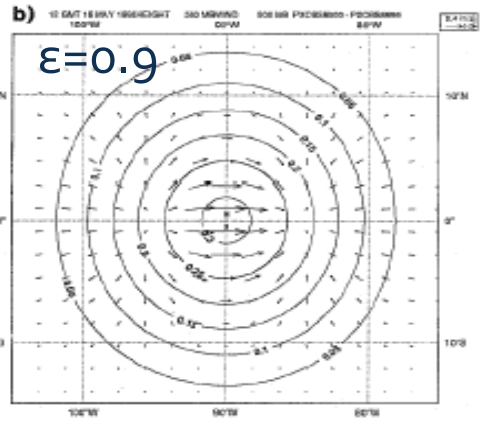

Potential impact of ADM-Aeolus in the tropics: Rossby wave example

Truth: ER n=1

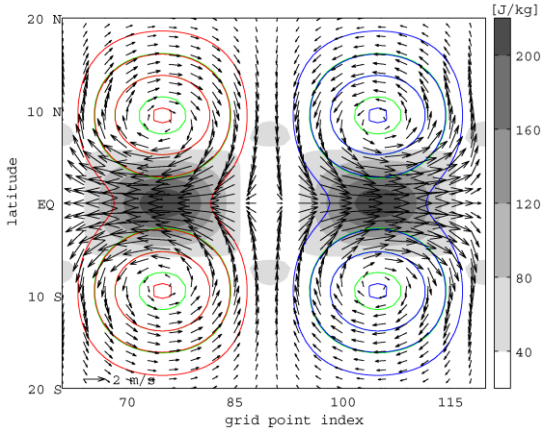

Reliable bkg-error variance spectrum

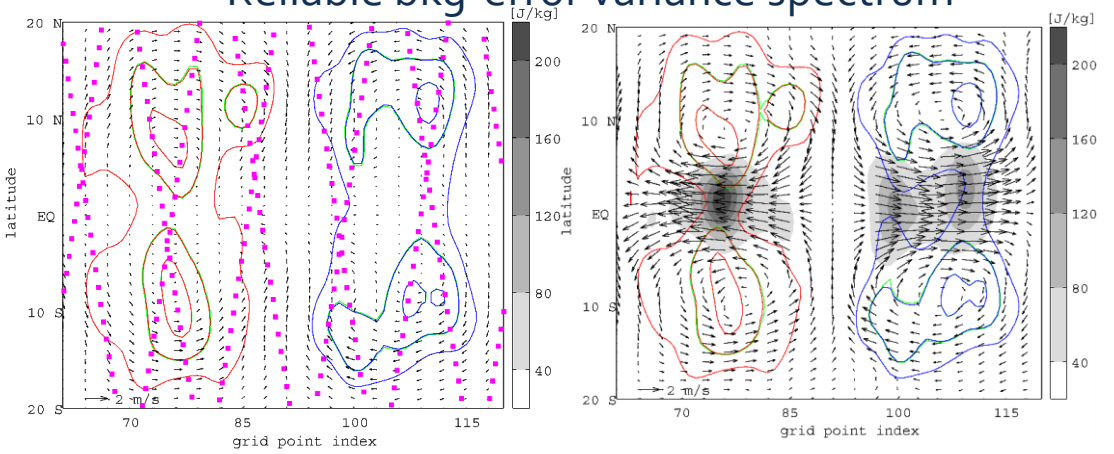

Poor bkg-error variance spectrum

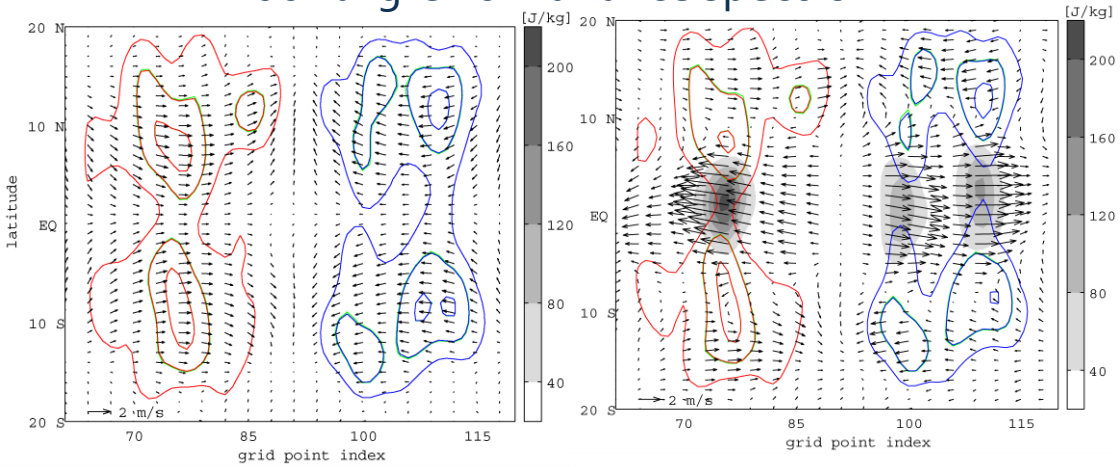

The spectrum of forecast error variance of the day is very important in the tropics

Žagar et al.,MWR 2008

3. Scale-dependent and flow-dependent growth of tropical forecast errors

Representation of the global error covariances using Hough functions

$$\mathbf{B} \approx \frac{1}{N_{\text{ens}} - 1} \sum_{i=1}^{N_{\text{ens}}} \Delta \mathbf{x}_i^B \cdot (\Delta \mathbf{x}_i^B)^{\mathrm{T}}$$

Estimate of the bkg error from the ensemble

$$\chi = \mathbf{L}\Delta \mathbf{x}^B$$

$$\mathbf{L} = \mathbf{D}\Theta_{\varphi}\mathbf{F}_{\lambda}\mathbf{G}_{m}$$

G_y – projection on the vertical structure
Θ – projection on the meridionally part of Hough harmonics
D – spectral variance density normalization
F – Fourier transform in the zonal direction

$$\mathcal{S}_\chi = \frac{1}{2}\ln\det(\mathbf{LBL}^{\mathrm{T}}) - \frac{1}{2}\ln\det(\mathbf{LAL}^{\mathrm{T}})$$

Entropy reduction M. Fisher, 2003

$$\approx \frac{1}{2}\ln\prod_{\nu=1}^{N}\frac{[\gamma_\nu^B]^2}{[\gamma_\nu^A]^2} \approx \frac{1}{2}\sum_{\nu=1}^{N}\ln\frac{[\gamma_\nu^B]^2}{[\gamma_\nu^A]^2}$$

$$\mathcal{S}_\chi = \frac{1}{2}\sum_{\nu=1}^{N}\ln\mathcal{I}_\nu^{-1}$$

$$\mathcal{I}_\nu = \mathcal{I}_n^k(m) = \frac{[\gamma_\nu^A]^2}{[\gamma_\nu^B]^2}$$

Fc-error variance reduction

Žagar et al.,MWR 2016

Decomposition of the ensemble spread in balanced and unbalanced (IG) parts

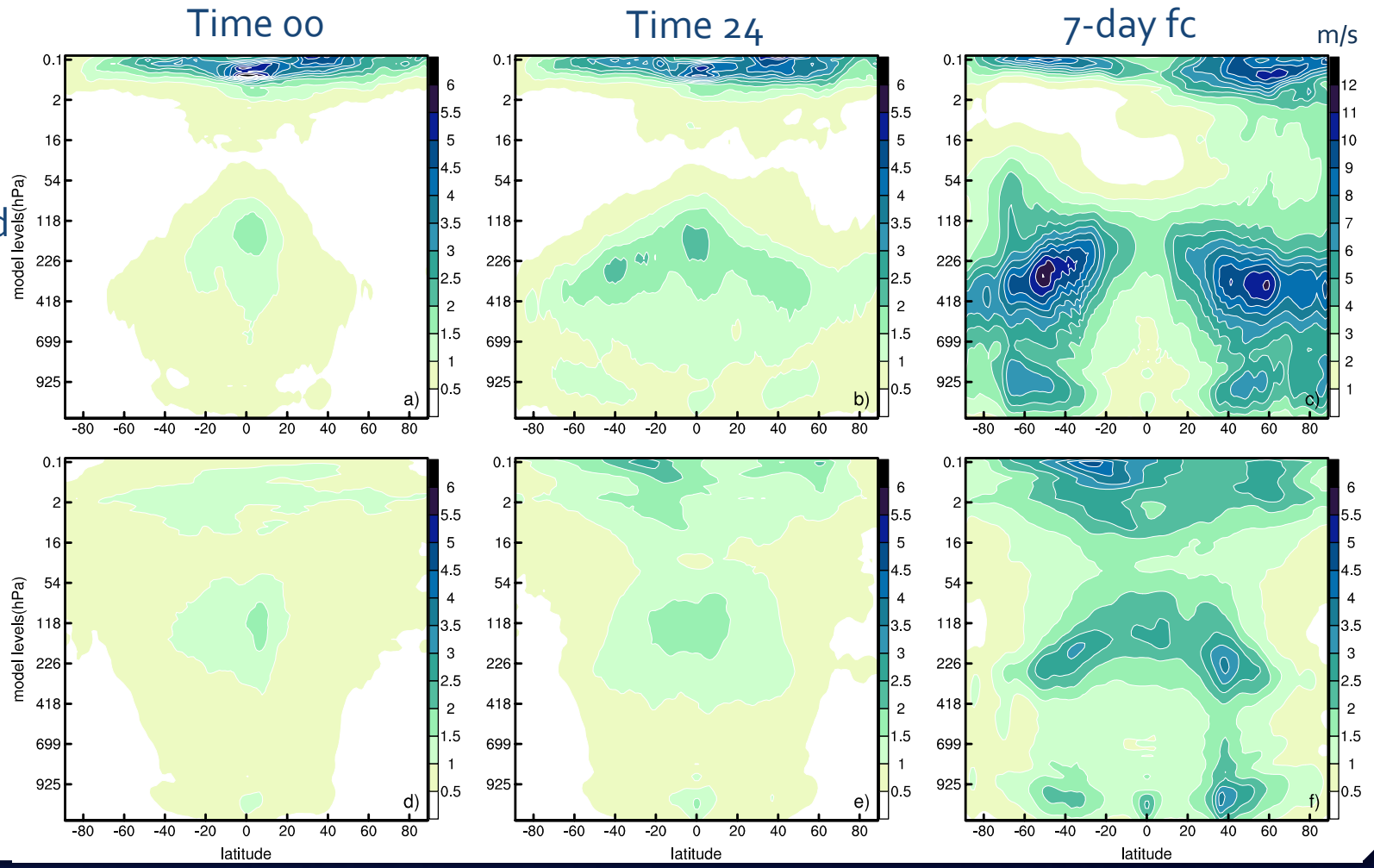

Short-range forecast error statistics, EDA

12-hr fc range

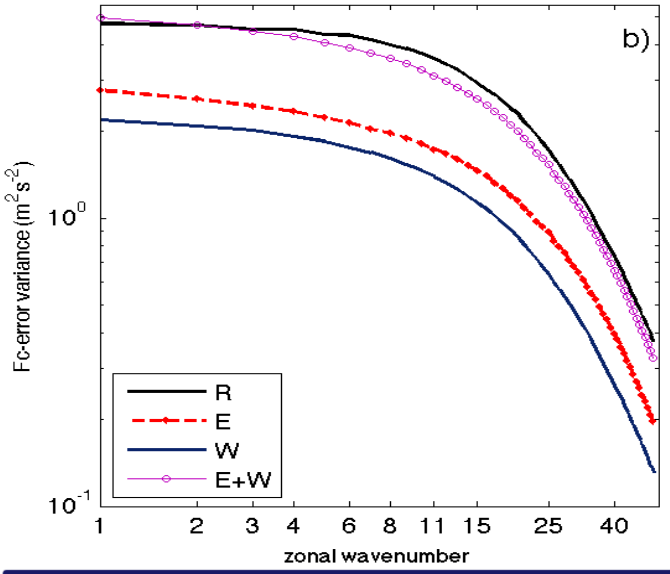

ROT	EIG	WIG
~52%	~27%	~21%

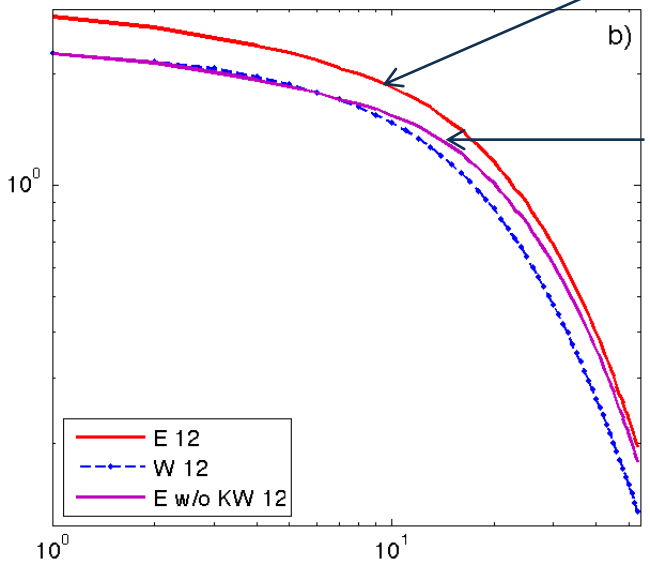

Kelvin waves make about 15% of EIG fc-error variance

Almost half of the variance in short-term forecast errors is associated with the inertio-gravity modes. EIG dominates over WIG on all scales. Data from July 2007.

Flow dependency of the simulated forecast errors in EDA

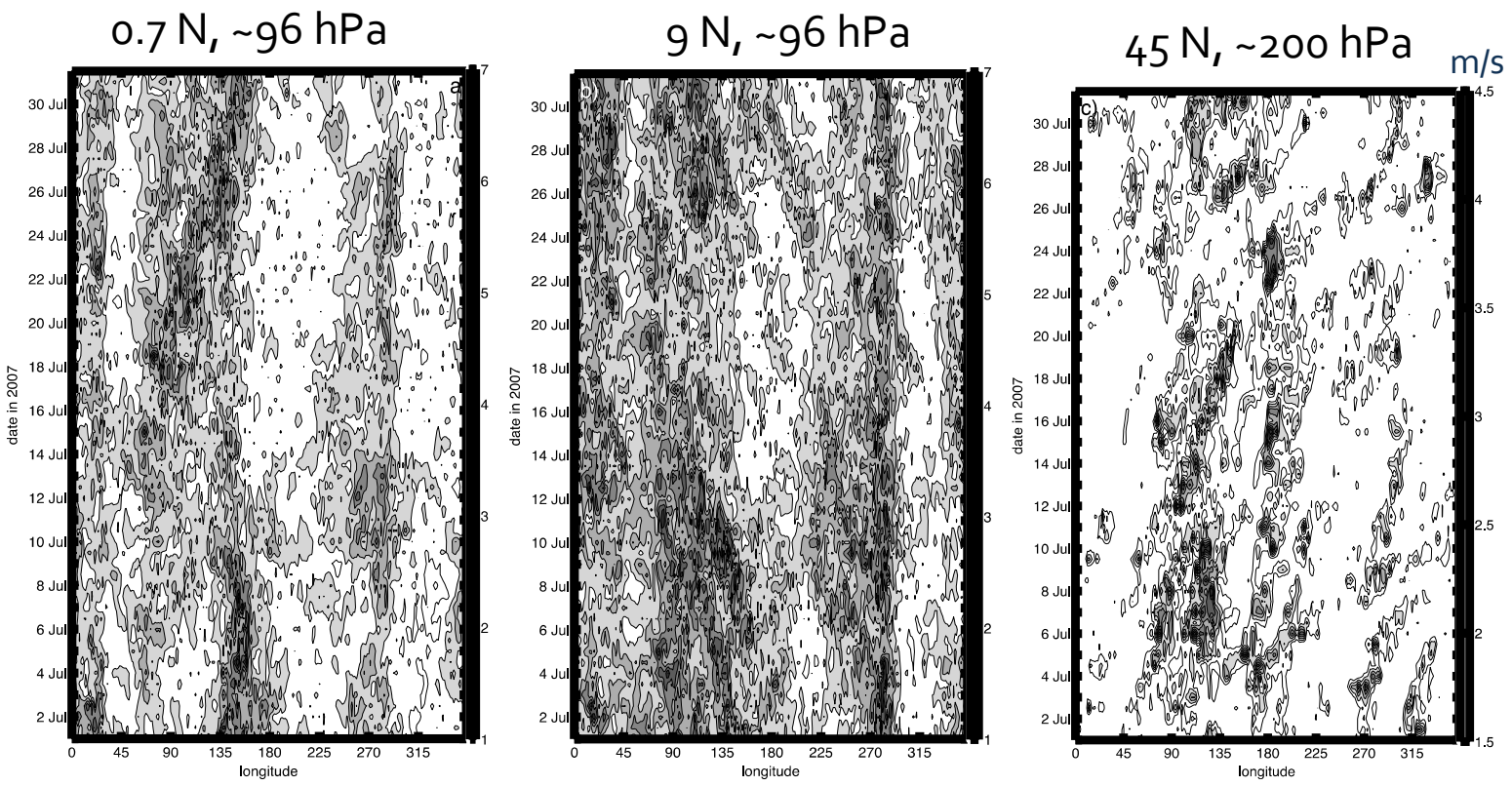

3-h fc errors in the zonal wind, derived from the ECMWF ensemble (cy32r3) during 1 month (July 2007)

Žagar et al., 2013, QJRMS

Short term growth of simulated forecast errors in EDA in relation to flow

[Variance(12) – Variance(3)] / Variance(3)*100%

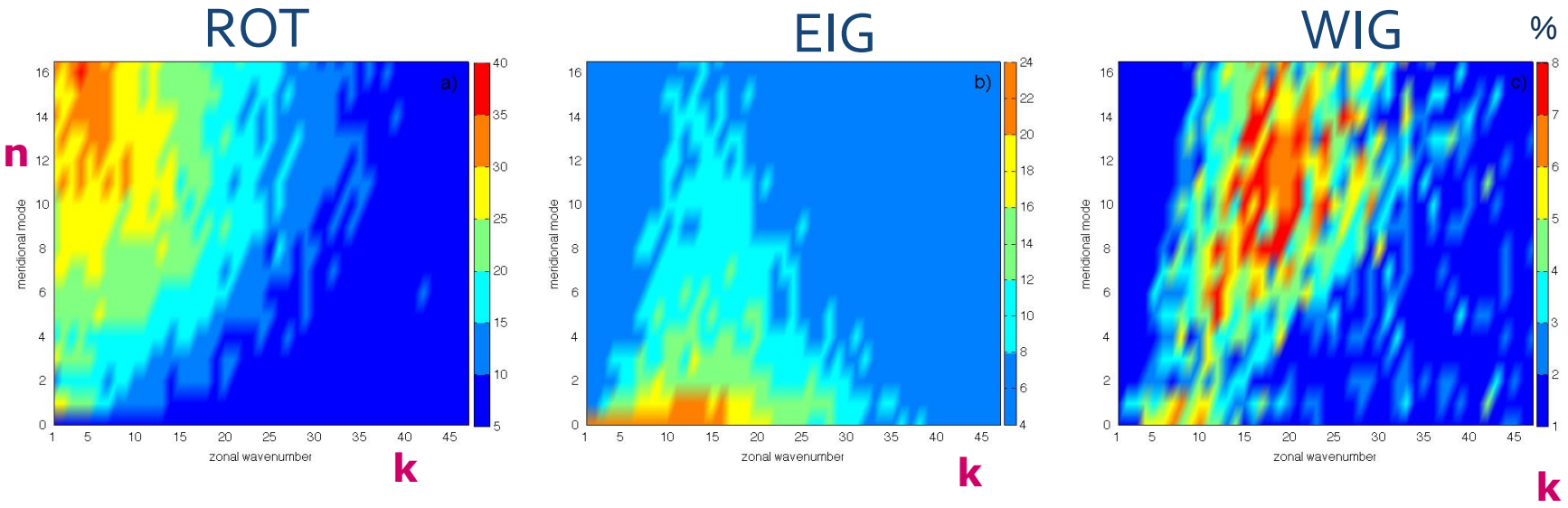

In the tropics, the short-range growth is largest in the Kelvin mode
The growth in WIG modes is accompanying the balanced variance growth in the midlatitudes

Žagar et al., 2013, QJRMS

Flow dependent growth of forecast uncertainties in ENS

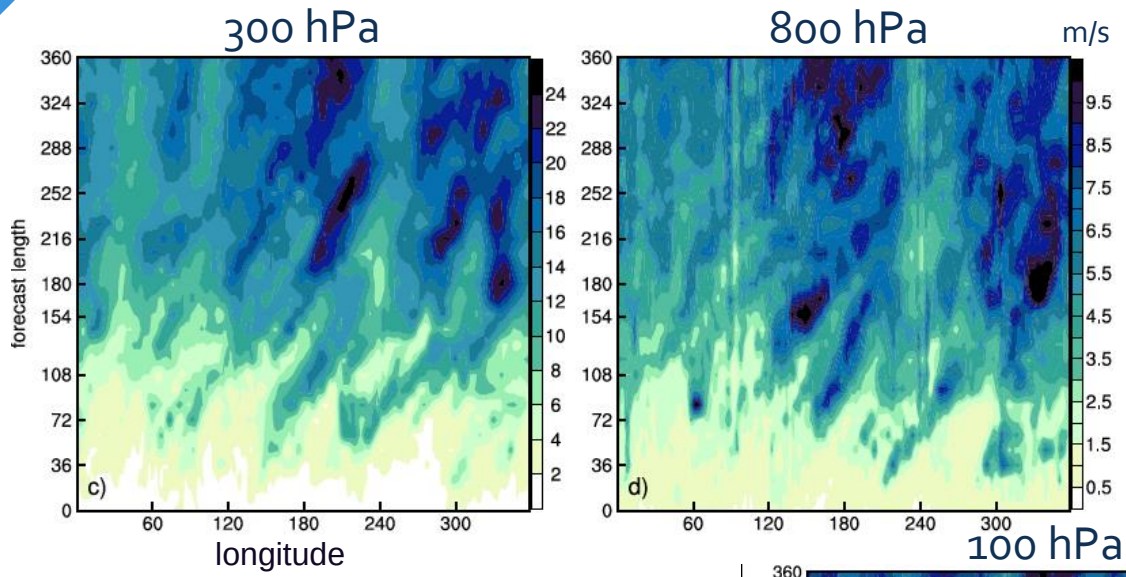

Mid-latitudes 45 N

Zonal wind (m/s)

Ensemble spread

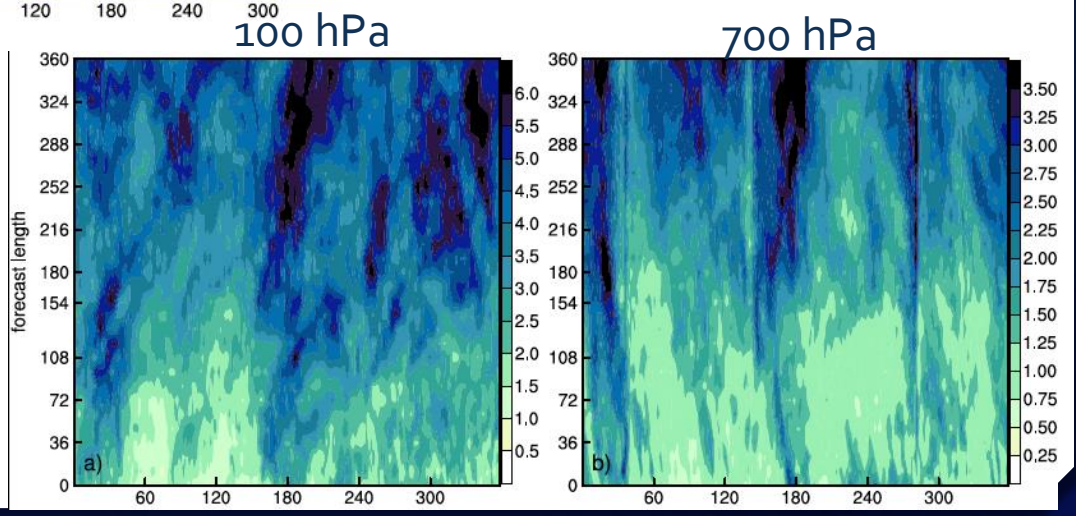

Tropics, 0.7 S

Zonal wind (m/s)

Ensemble spread

2 Apr 2016, 00 UTC, ECMWF ENS

Growth of the spread w.r.t. initial spread as a function of the zonal scale

Balanced spread

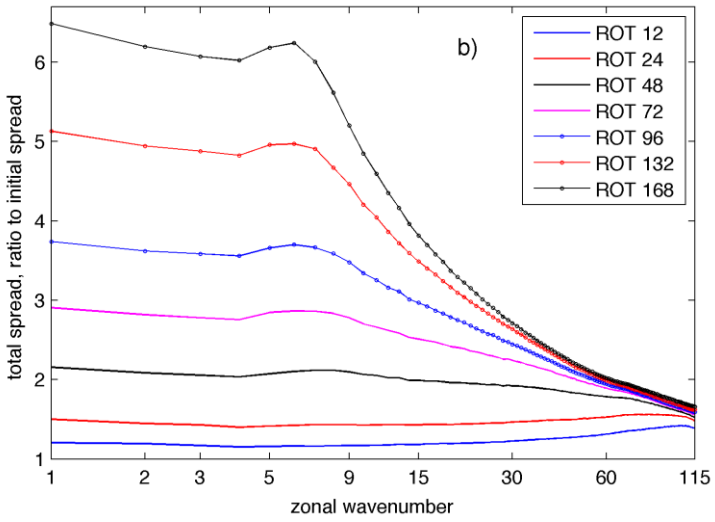

IG spread

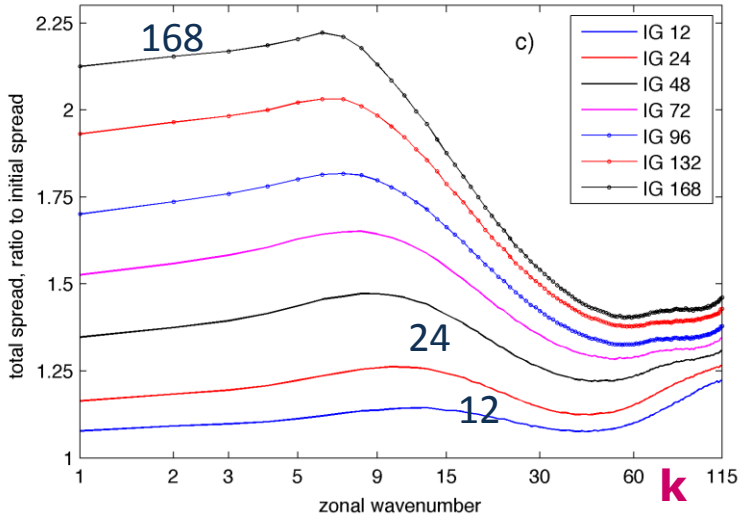

Dataset: operational ENS in Dec 2014

Initially, the growth of spread is largest in the smallest scales and the synoptic scales of the IG modes (tropics).

Žagar et al., 2015, JAS

Growth of the spread w.r.t. initial spread as a function of zonal scale

WIG spread

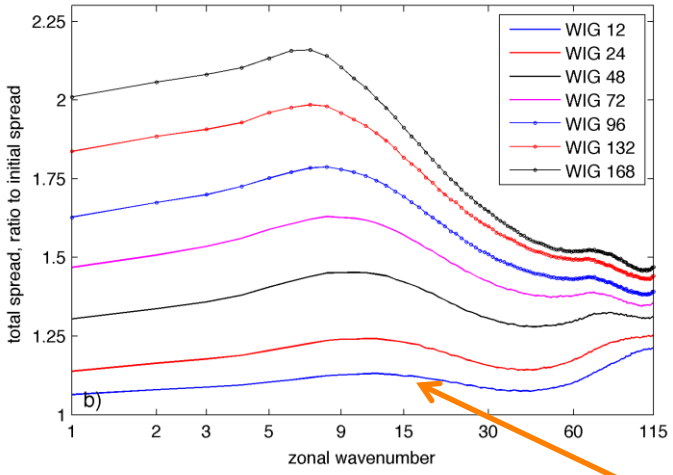

EIG spread

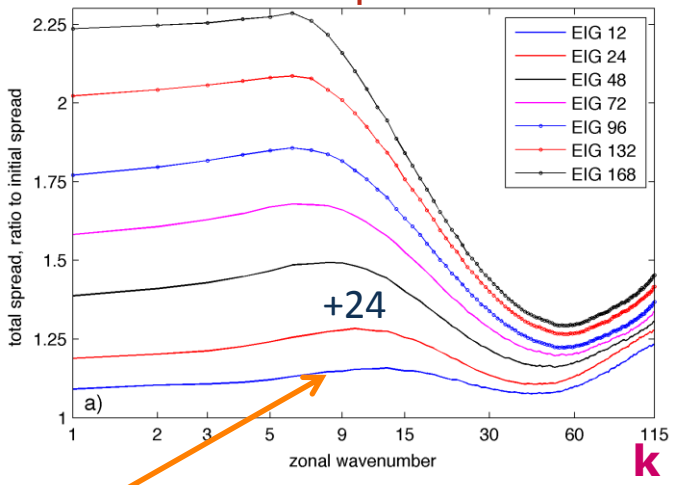

IG spread

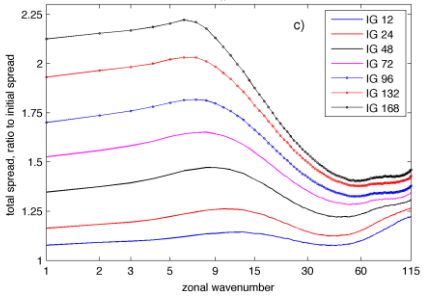

Žagar et al., 2015, JAS

Growth of the spread w.r.t. initial spread as a function of the zonal scale

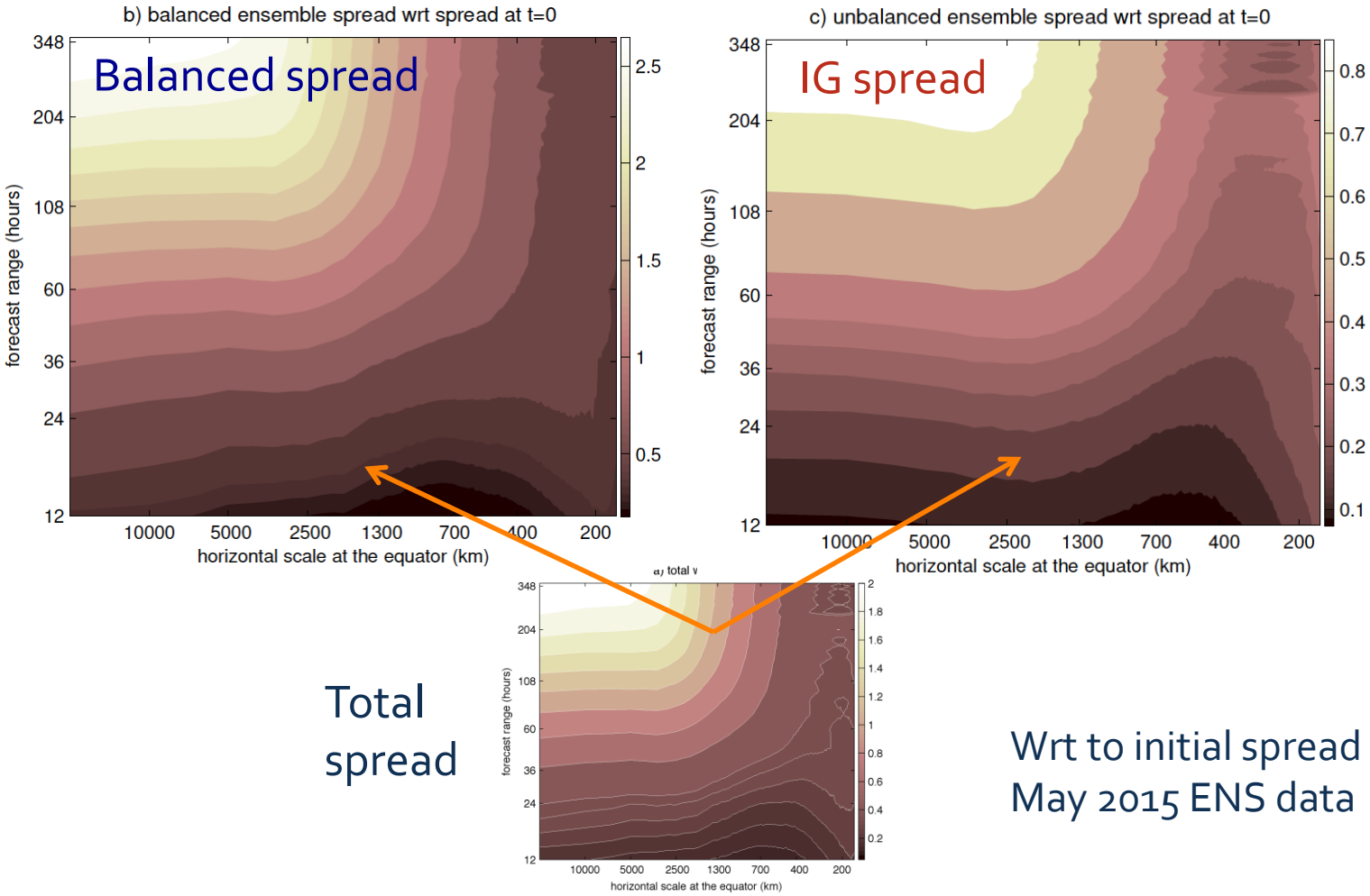

Wrt to initial spread
May 2015 ENS data

Scale-dependent limits of the growth of spread in ENS

Lorenz, 1984

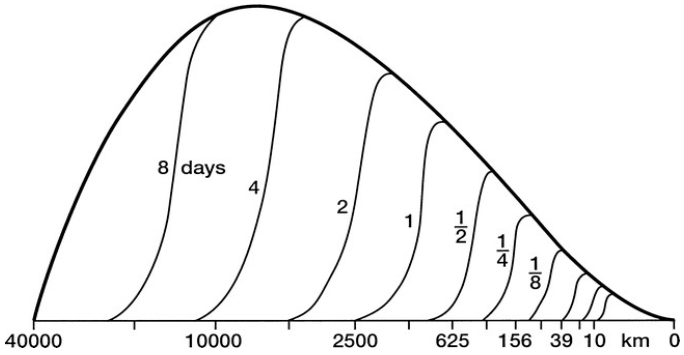

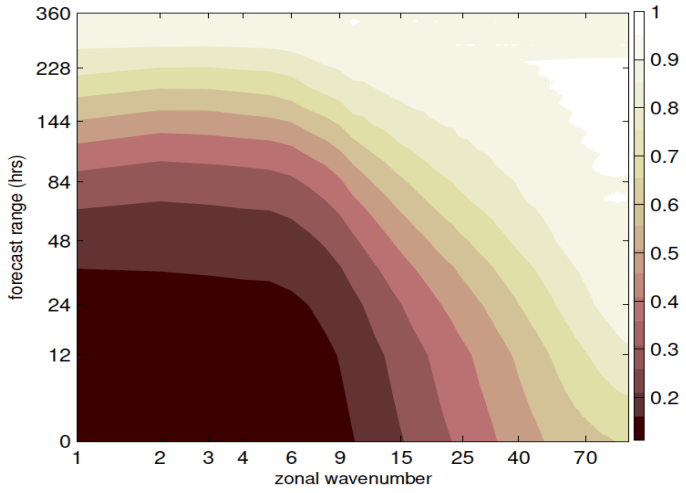

Dalcher and Kalnay, 1987

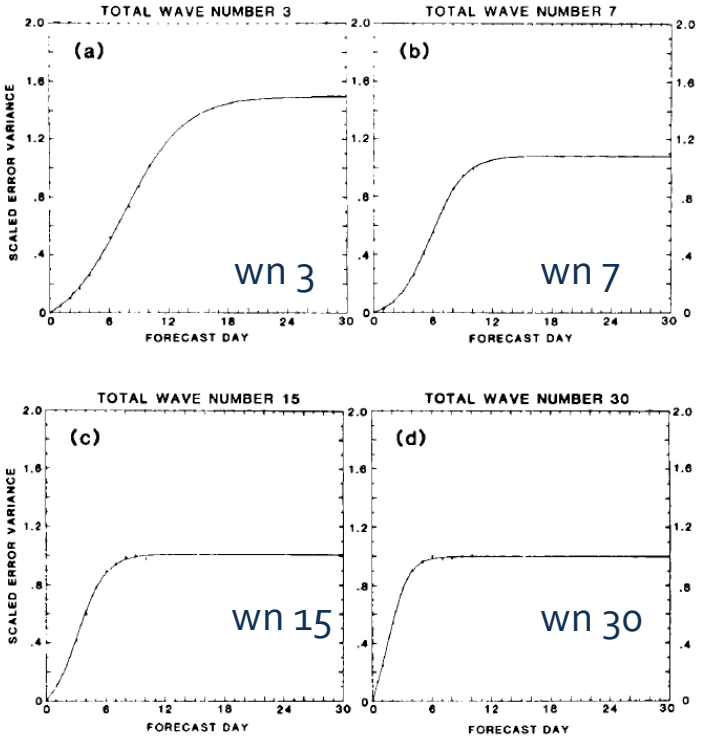

Growth of error variance for Z500 in the ECMWF model in early 1980s. The smaller the scale, the shorter the predictability limit

Scale and flow dependent representation of the ensemble reliability

Dec 2014,
Operational ENS data

A lack of variability is initially seen in subsynoptic balanced scales, and lateron in tropical IG modes, primarily the Kelvin mode

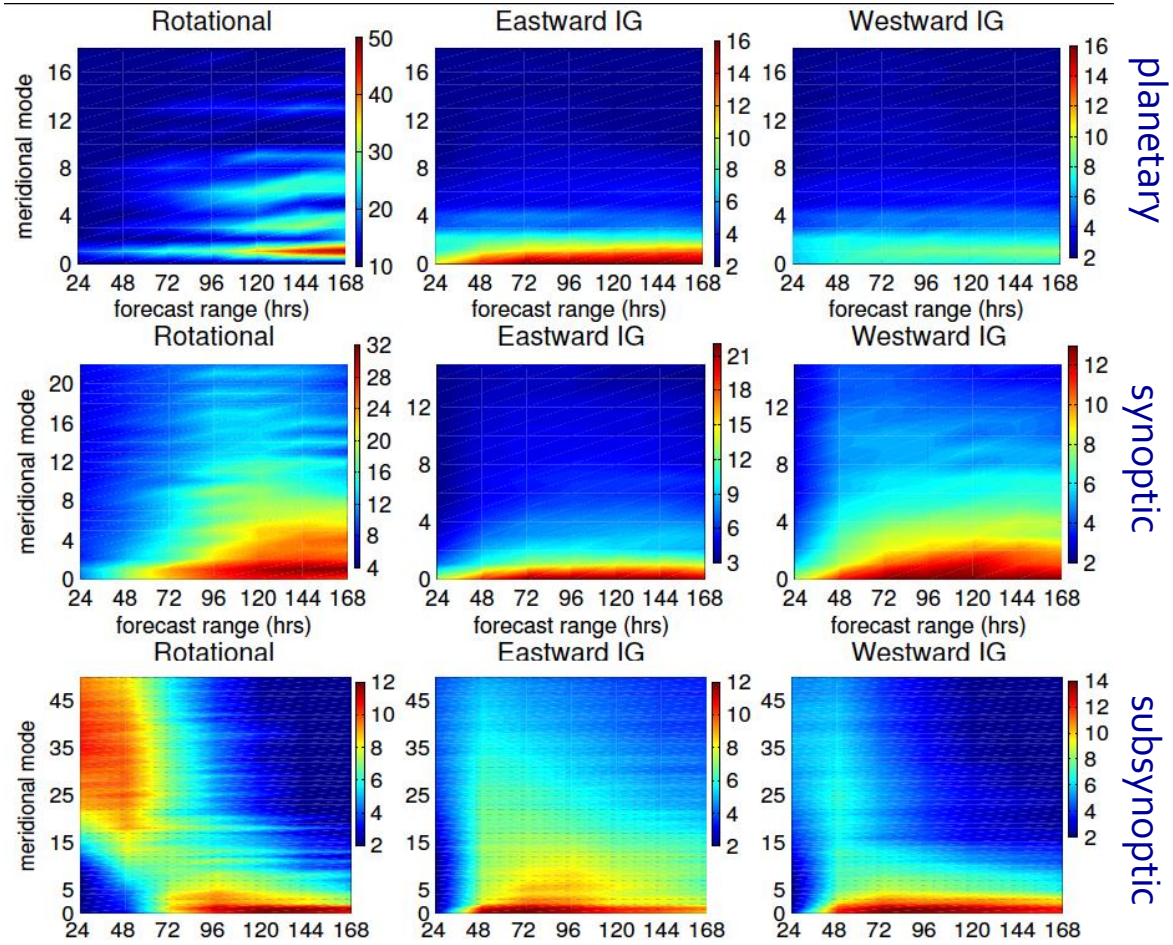

Žagar et al., 2015, JAS

4. Role of observations and model error in tropical uncertainties

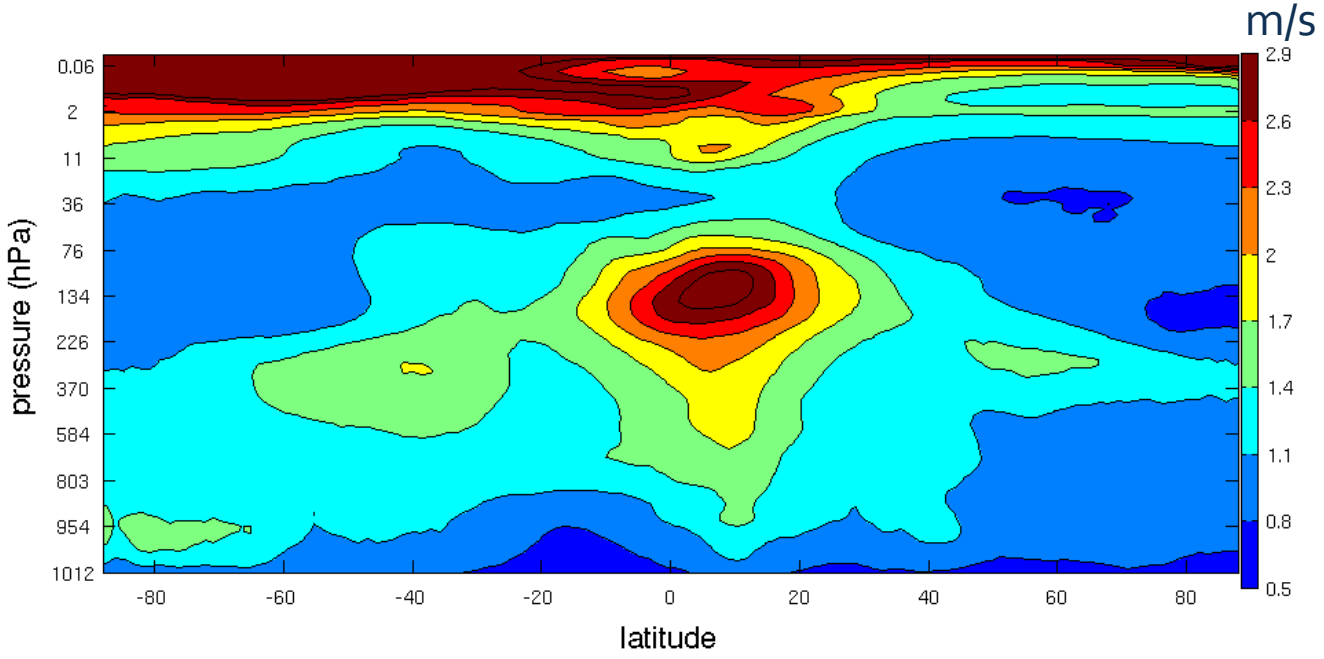

Analysis and forecast uncertainties in OSSE with a perfect model

Data Assimilation Research Testbed (DART), by Jeff Anderson and collaborators, *http://www.image.ucar.edu/DAReS/DART/*

Spectral T85 Community Atmosphere Model, CAM 4 physics

Long spin-up (from 1 Jan 2008) with the observed SST to reproduce nature run ('truth')

Preparation of the observations from the nature run

Preparation of the homogeneous observing network (Δ~920 km)

Assimilation cycle during three months (Aug-Oct) in 2008

No inflation

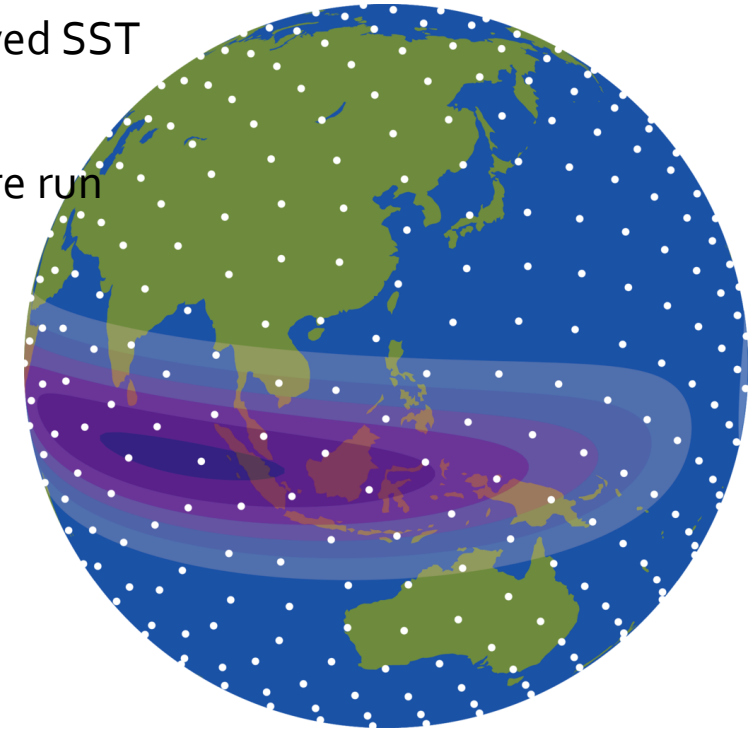

Žagar et al., 2016, MWR

Short-range global forecast errors in the perfect-model EnKF framework

pr, zonal wind m/s

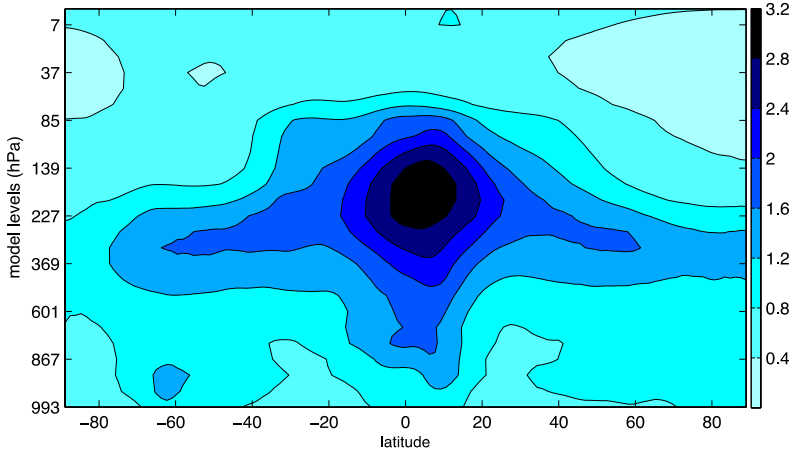

Spread of 12-hr forecast ensemble
3-month average

(pr-po)/pr, zonal wind %

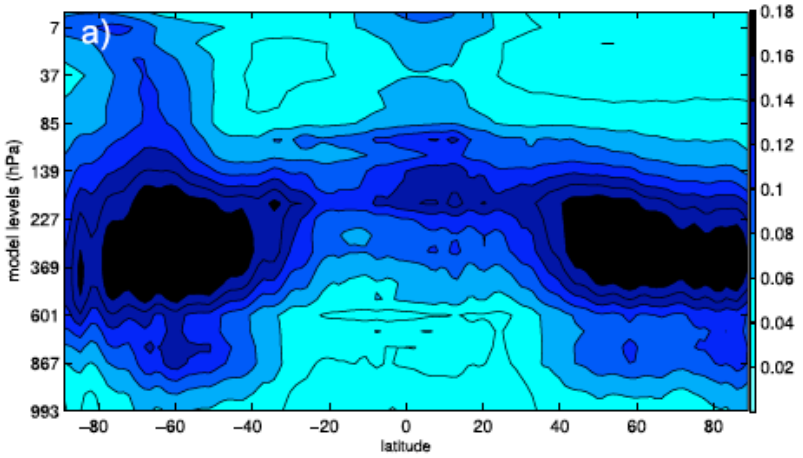

Prior – posterior ensemble spread in each (x,y,z), averaged in time and zonally

Perfect model vs. NWP model

Perfect model exp

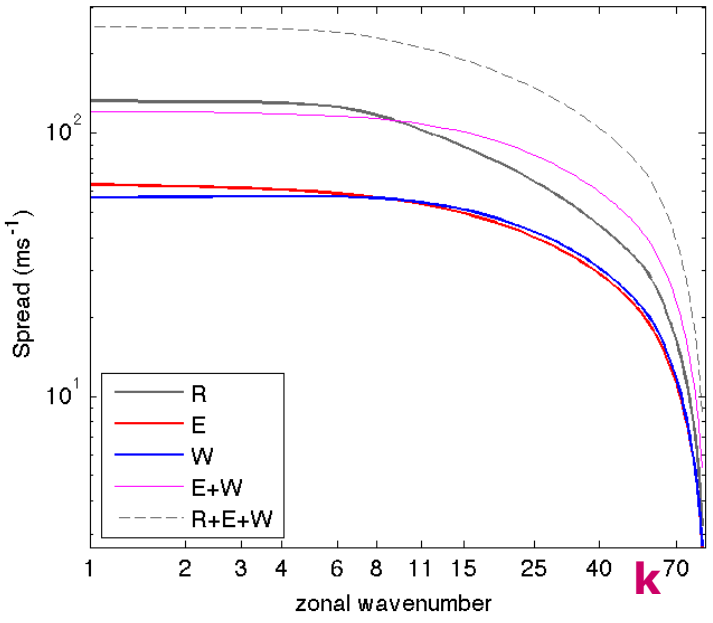

ECMWF EDA

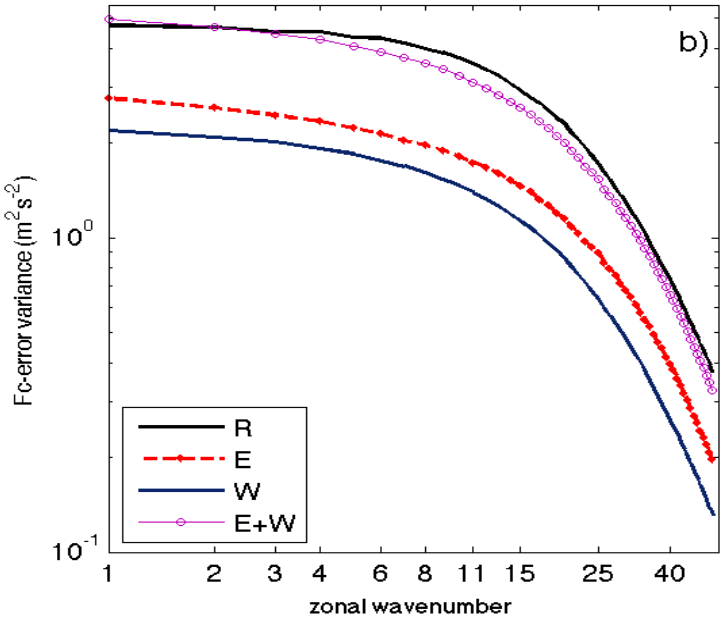

Data assimilation is not efficient in reducing the tropical large scale spread, not even in the perfect model framework

Scale-dependency of the 12-hr forecast error variances in EnKF with a perfect model

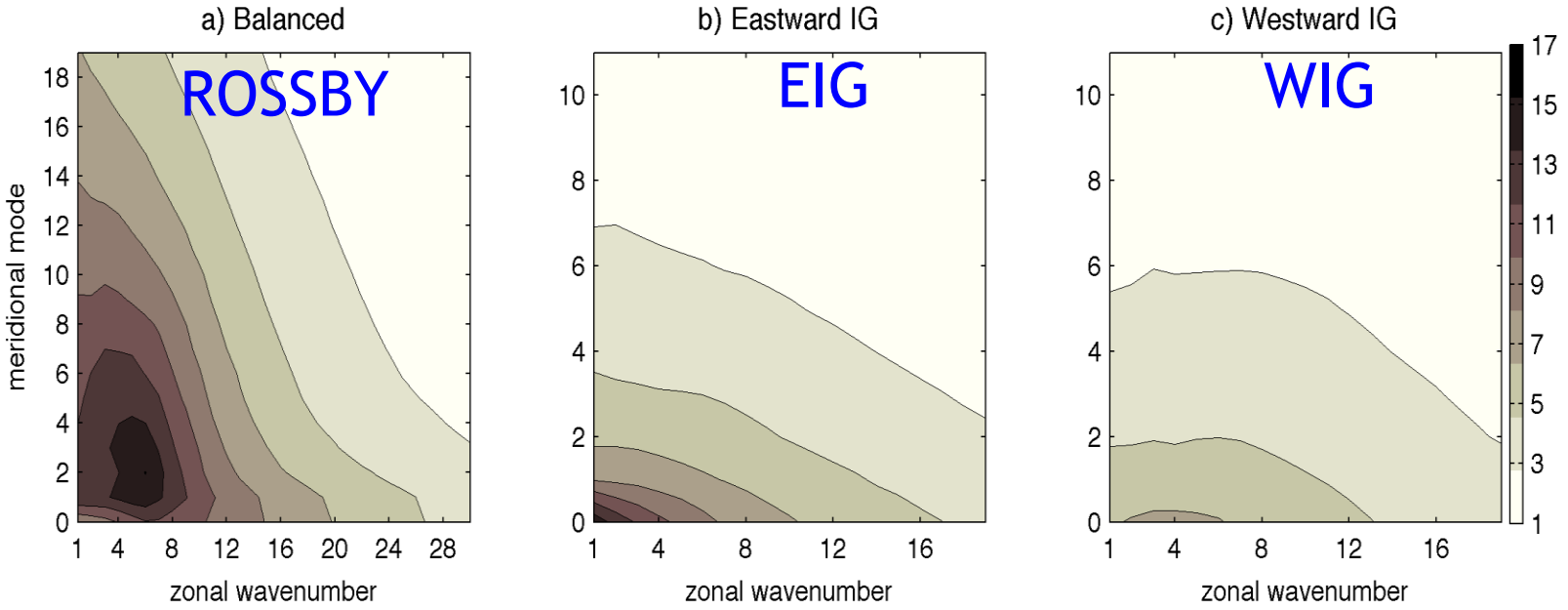

Distribution of the variance in analysis ensmeble looks very similar. As expected, largest variance is in synoptic scales and balanced modes (mid-latitudes) and in the large-scale Kelvin wave

Žagar et al., 2016, MWR

Data assimilation efficiency: variance reduction

Efficiency = (po-pr)/pr

ROSSBY

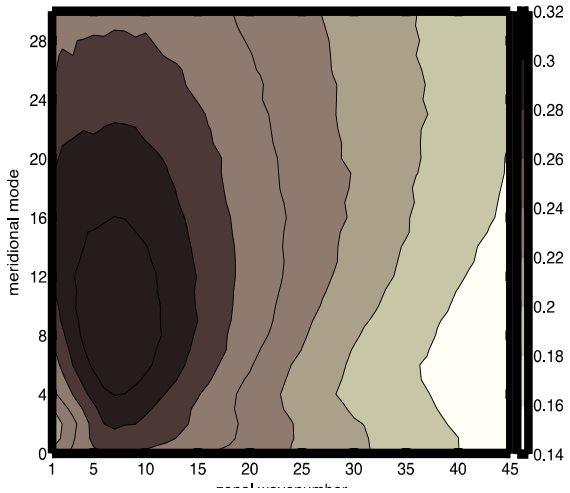

EIG

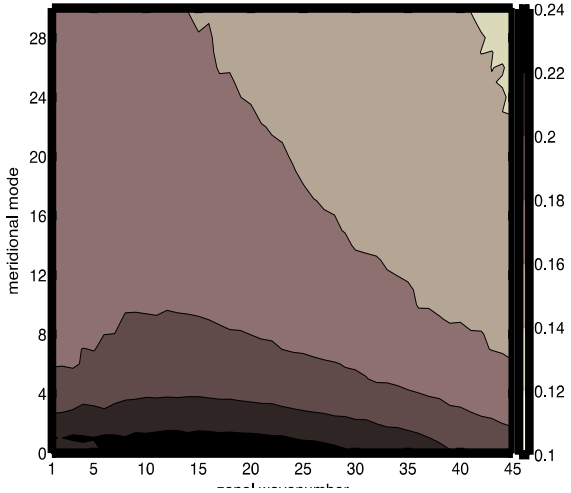

WIG

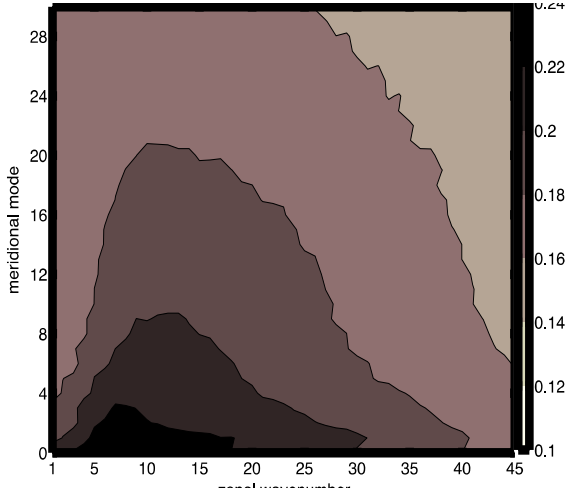

The assimilation is most efficient in synoptic scales, for both balanced and IG motions

Žagar et al., 2016, MWR

Data assimilation efficiency: variance reduction

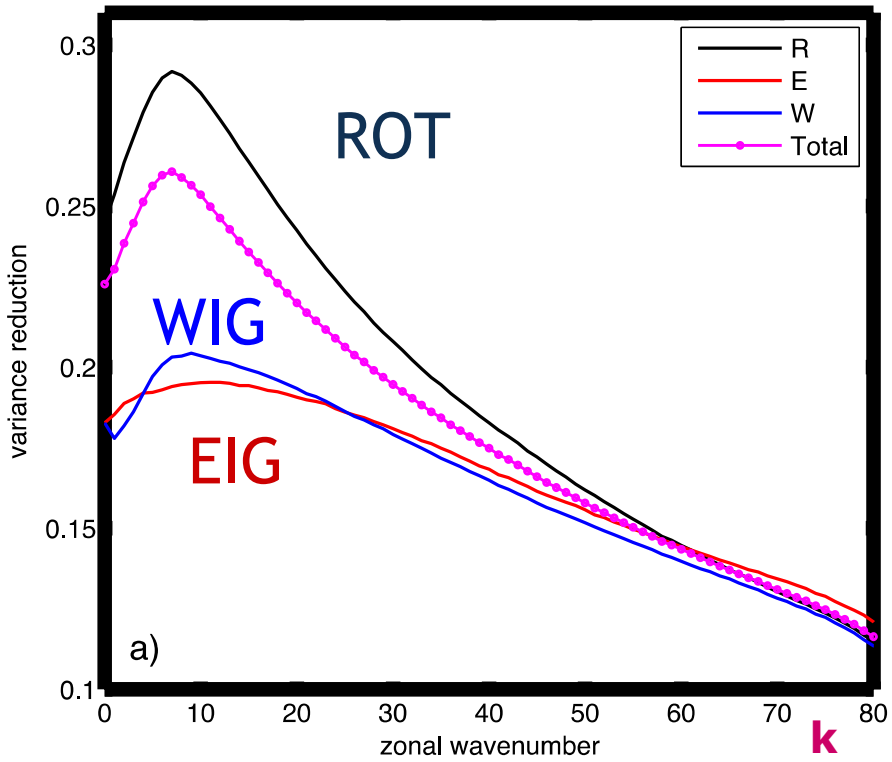

Efficiency = variance reduction as a function of zonal wavenumber

The assimilation is most efficient in synoptic scales, for both balanced and IG motions but much more efficient for balanced.

Covariance localization radius was 0.2 (around 1300 km at Eq).

Žagar et al., 2016, MWR

Impact of the covariance localization radius

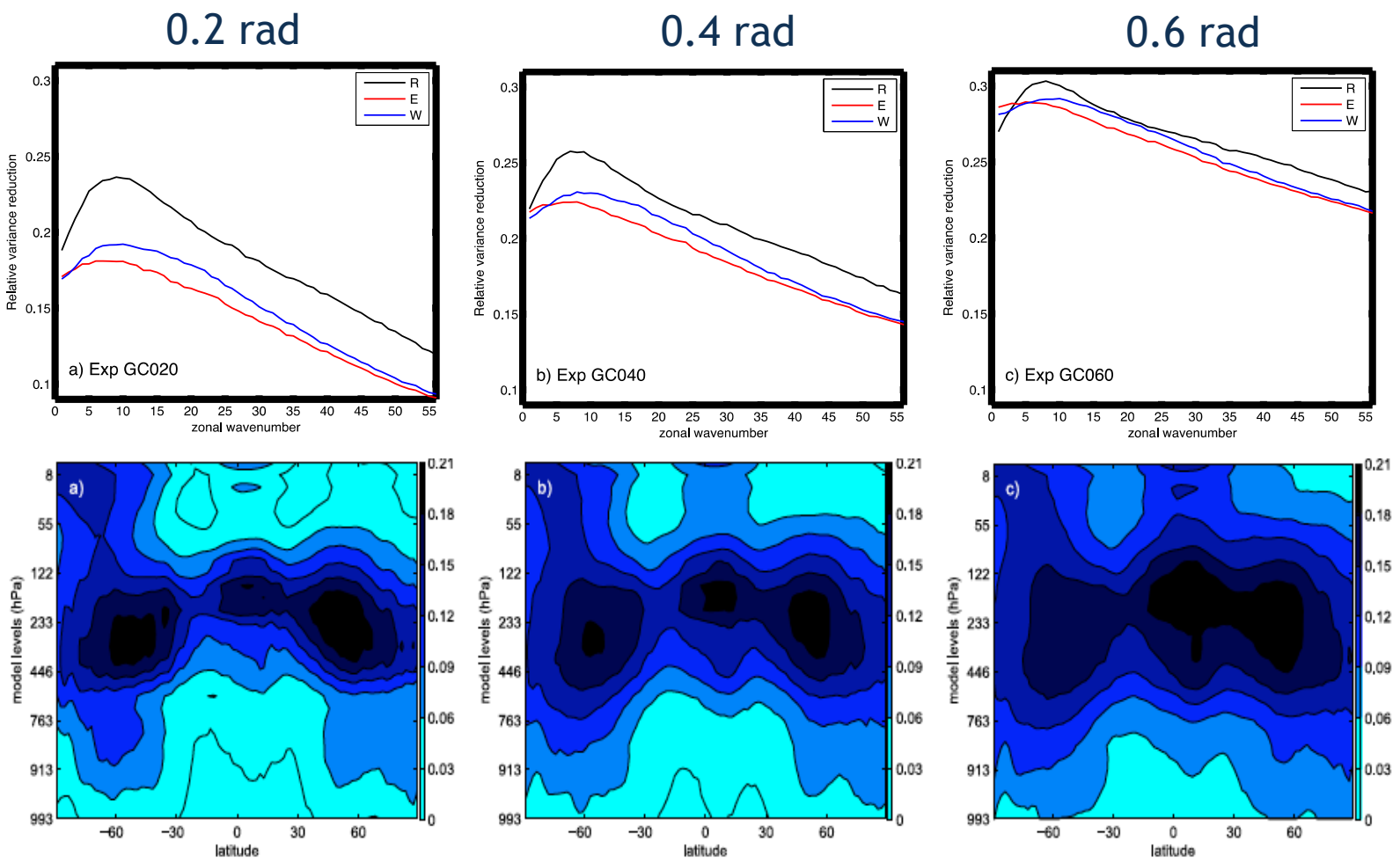

Summary

- Tropics are characterized by largest analysis uncertainties and largest growth of forecast uncertainties during the first 24-36 hours in the IFS system.
- The uncertainties are on average largest on the largest scales.
- Uncertainties are flow dependent. Uncertainties in wind and geo. height fields in the tropics are balanced about 50%.
- Maximal short-range forecast uncertainties in the tropical upper troposphere have not been reduced using a perfect model with an EnKF. Covariance localization radius is very important in the tropics.
- Introducing a mass-wind constraint based on large-scale equatorial waves may be helpful.

Thank you for your attention!

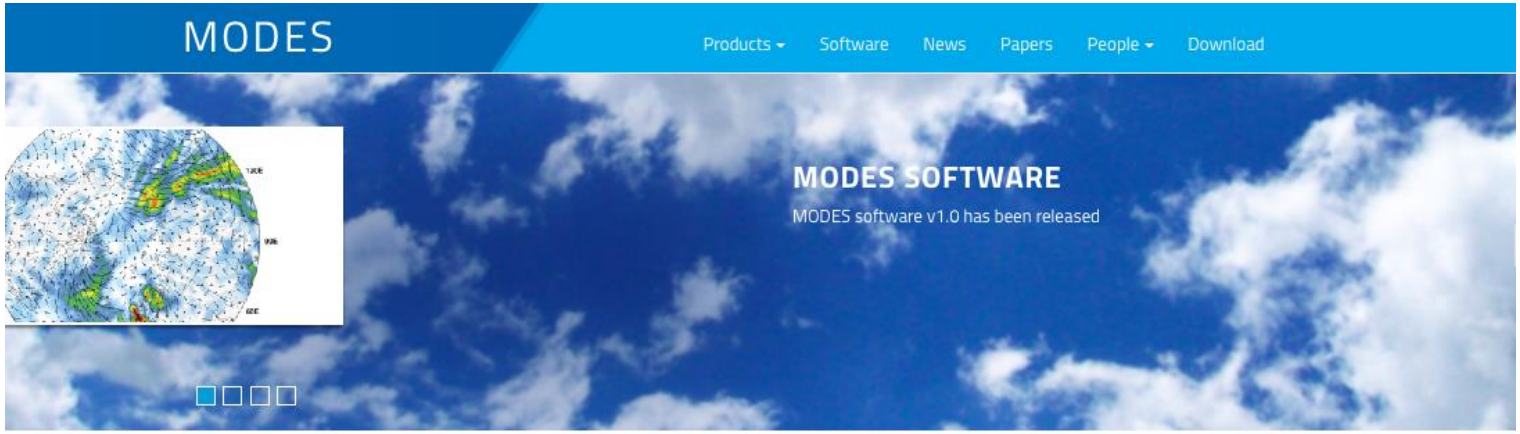

Modal view of atmospheric circulation

MODES focuses on the representation of the inertio-gravity circulation in numerical weather prediction models, reanalyses, ensemble prediction systems and climate simulations. The project methodology relies on the decomposition of global circulation in terms of 3D orthogonal normal-mode functions. It allows quantification of the role of inertio-gravity waves in atmospheric variability across the whole spectrum of resolved spatial and temporal scales.

MORE ABOUT MODES

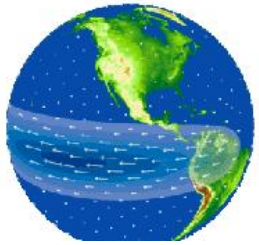

http://meteo.fmf.uni-lj.si/MODES

erc